Lagrangian Transport Calculations Using *UARS* Data. Part I: Passive Tracers

G. L. MANNEY,* R. W. ZUREK,* W. A. LAHOZ,† R. S. HARWOOD,# J. C. GILLE,@ J. B. KUMER,&
J. L. MERGENTHALER,& A. E. ROCHE,& A. O'NEILL,† R. SWINBANK,** AND J. W. WATERS*

*Jet Propulsion Laboratory/California Institute of Technology, Pasadena, California
†Centre for Global Atmospheric Modelling, Reading, United Kingdom
#Edinburgh University, Edinburgh, United Kingdom
@National Center for Atmospheric Research, Boulder, Colorado
&Lockheed Palo Alto Research Laboratory, Palo Alto, California
**Meteorological Office, Bracknell, United Kingdom

(Manuscript received 14 March 1994, in final form 14 February 1995)

ABSTRACT

The transport of passive tracers observed by the *Upper Atmosphere Research Satellite* is simulated using computed three-dimensional trajectories of ≈100 000 air parcels initialized on a stratospheric grid, with horizontal winds provided by the United Kingdom Meteorological Office data assimilation system, and vertical (cross isentropic) velocities computed using a fast radiation code. The conservative evolution of trace constituent fields is estimated over 20–30-day periods by assigning to each parcel the observed mixing ratio of the long-lived trace gases N_2O and CH_4 observed by the Cryogenic Limb Array Etalon Spectrometer (CLAES) and H_2O observed by the Microwave Limb Sounder (MLS) on the initialization date. Agreement between calculated and observed fields is best inside the polar vortex and is better in the Arctic than in the Antarctic. Although there is not always detailed agreement outside the vortex, the trajectory calculations still reproduce the average large-scale characteristics of passive tracer evolution in midlatitudes. In late winter, synoptic maps from trajectory calculations reproduce all major features of the observations, including large tongues or blobs of material drawn from low latitudes into the region of the anticyclone during February–March 1993. Comparison of lower-stratospheric observations of the CLAES tracers with the calculations suggests that discontinuities seen in CLAES data in the Antarctic late winter lower stratosphere are inconsistent with passive tracer behavior. In the Arctic, and in the Antarctic late winter, MLS H_2O observations show behavior that is inconsistent with calculations and with that expected for passive tracers inside the polar vortex in the middle-to-upper stratosphere. Diabatic descent rates in the Arctic lower stratosphere deduced from data are consistent with those from the calculations. In the Antarctic lower stratosphere, the calculations appear to underestimate the diabatic descent. The agreement between large-scale features of calculated and observed tracer fields supports the utility of these calculations in diagnosing trace species transport in the winter polar vortex.

1. Introduction

Observations of passive tracers are invaluable in diagnosing stratospheric air motions. Nitrous oxide (N_2O) measured by aircraft has been used to locate and describe the polar vortex and to estimate vertical velocities (Podolske et al. 1989; Loewenstein et al. 1990; Schoeberl et al. 1989, 1992; Strahan et al. 1994, and references therein). Manney et al. (1994a) used N_2O measurements from the Cryogen Limb Array Etalon Spectrometer (CLAES) on the *Upper Atmosphere Research Satellite (UARS)* to describe three-dimensional air motions during stratospheric warmings in February–March 1993, Lahoz et al. (1993, 1994) used CLAES N_2O and Microwave Limb Sounder (MLS) water vapor (H_2O) to examine vortex processes in the Northern Hemisphere (NH) midstratosphere, and Harwood et al. (1993) used MLS H_2O data to describe transport during spring in the Southern Hemisphere (SH). Manney et al. (1994b) used N_2O measurements in comparison with MLS ozone measurements to qualitatively separate chemical and dynamical effects in the NH lower stratosphere. Schoeberl et al. (1995) used methane (CH_4) and hydrogen fluoride (HF) measured by the *UARS* Halogen Occultation Experiment (HALOE) to deduce vertical velocities in the Antarctic lower stratosphere during October 1992.

Trajectory calculations provide another means of investigating air motions. Isentropic trajectory calculations (Bowman 1993; Chen et al. 1994; Chen 1994; Dahlberg and Bowman 1994) using winds derived from data have been used to study the degree of separation and mixing between polar vortex and midlatitude air during winter in the lower stratosphere of both hemispheres. Pierce and Fairlie (1993) used winds from a general circulation model to examine mixing at the vortex edge in the Arctic winter. Fisher et al. (1993) used three-dimensional winds from a mechanistic model of the stratosphere and mesosphere to describe

Corresponding author address: Dr. Gloria Manney, Jet Propulsion Laboratory, Mail Stop 183-701, 4800 Oak Grove Dr., Pasadena, CA 91109-8099.

the general features of large-scale air motion through the course of an SH winter. Manney et al. (1994c) used horizontal winds from the U.K. Meteorological Office (UKMO) data assimilation system and vertical velocities computed with a middle atmosphere radiation code to examine three-dimensional air motions and the mixing of polar and midlatitude air for recent winters in both the NH and the SH. These three-dimensional calculations have shown that trajectory calculations can simulate large-scale air motion for periods of several months.

Recent studies combine trajectory calculations and measurements of passive tracers to gain further insights into stratospheric air motions. Pierce et al. (1994) initialize clusters of trajectories at the sunrise/sunset HALOE measurement locations and assign to them the mixing ratio of trace species measured there. These parcels are then advected forward in time on an isentropic surface using UKMO horizontal winds to "fill in" the relatively sparse coverage provided by HALOE solar occultation measurements and to predict fields where HALOE did not measure. Morris et al. (1995) applied a similar technique to CLAES, HALOE, and MLS data by adding parcels to isentropic trajectory calculations at measurement locations and times, using winds calculated from National Meteorological Center data. In this case, the air motion predicted by the trajectory calculation is used to simulate a higher-resolution field than can be retrieved directly from *UARS* observations. Both studies focus on using the available meteorological information to enhance the resolution and/or extend the coverage of measurements, in effect as a mapping technique. Furthermore, numerical calculations show that even the use of coarse-resolution wind fields to compute advection (whether Lagrangian or Eulerian) can successfully simulate higher-resolution features of trace species distributions (e.g., Hsu 1980; Waugh et al. 1994; O'Neill et al. 1994; Sutton et al. 1994).

The use of trajectories to compute tracer advection has certain practical advantages. First, they provide a good means of visualizing the air motions in general, as shown by Manney et al. (1994c) and O'Neill et al. (1994). In part, this is due to the fact that the trajectory calculations can generate synoptic- and subsynoptic-scale features of the tracer distributions (e.g., long thin filaments of air being drawn off the polar vortex), even when the initial (remotely observed) fields, and the input wind fields, are of relatively coarse resolution (e.g., Waugh et al. 1994). Second, the trajectories are computed once and for all, for a given period. Besides being computationally efficient, this permits the same "transport" to be tested with several observed trace gas fields, each with its different spatial distribution and measurement error, thereby providing greater confidence that the transport is approximately right. A difficulty in using trajectory calculations to study tracer transport is the lack of uniformity in the resultant fields, making additional manipulation of the results or the data necessary to make comparisons. Another possible disadvantage is the lack of any parameterization of small-scale mixing.

Here we use three-dimensional calculations of air parcel motion throughout the stratosphere and observations of passive tracers from the CLAES and MLS instruments on *UARS* to examine and compare the transport of passive tracers. This approach is different from those taken in the above-mentioned studies in that we initialize a three-dimensional grid of parcels on a given day with tracer mixing ratios taken from gridded *UARS* fields having nearly global coverage on a daily basis. Those parcels are then advected in three dimensions using UKMO horizontal wind fields and vertical velocities from a radiation calculation. This is in effect a kind of transport code, but one in which, besides examining the large-scale evolution of regridded fields, we can also examine the relatively high-resolution picture given by the trajectory calculations. We are particularly interested in the winter polar regions, since the understanding of transport effects there, gained by examining passive tracers, will allow us to begin separating dynamical from chemical effects for chemically active species such as ozone.

Here, we examine and contrast results computed for the 1992–93 northern winter and the 1992 southern winter, during periods from which both CLAES and MLS data are available. Because of the 57° inclination of the *UARS* orbit and its precession in local time, the latitude coverage achieved by CLAES and MLS alternates between 34°S to 80°N and 80°S to 34°N approximately every 36 days. During December 1992, February–March 1993, and August 1992, measurements of N_2O and CH_4 from CLAES, and H_2O from MLS, are available in the winter hemisphere. Although solar array drive anomalies in early June 1992 cause most *UARS* instruments to be turned off, during the latter half of June N_2O and CH_4 from CLAES are available on most days. The availability of several tracers provides a means of testing our calculations of passive tracer motions and can also identify possible times or regions where there are inconsistencies in the data. The two late winter time periods are of particular interest since they are both times when observed ozone decreases in the lower stratosphere have been ascribed to chemical loss (Waters et al. 1993a,b; Manney et al. 1993; Manney et al. 1994b).

2. Data and analysis

a. Trajectory calculations

The trajectory calculations are initialized as described by Manney et al. (1994c), but the previous hemispheric coverage of initial parcel positions has been extended in latitude to 20° in the hemisphere opposite to the one of interest, so that cross-equatorial flow does not result in a lack of parcels at low latitudes. Parcels are initialized on a 2° latitude by 5° longitude

grid and at 26 potential temperature levels throughout the stratosphere: 400, 420, 440, 465, 490, 520, 550, 585, 620, 655, 690, 740, 790, 840, 900, 960, 1030, 1100, 1170, 1250, 1320, 1400, 1520, 1650, 1750, and 1850 K. Horizontal winds are from the UKMO data assimilation system (Swinbank and O'Neill 1994) and, since diabatic heating rates from the UKMO assimilations are not available as an output product, vertical velocities are obtained from a recent version of the middle atmosphere radiation code MIDRAD, an earlier version of which is described by Shine (1987). Temperatures in the radiation code are from the UKMO data; the runs here are restricted to times when MLS and CLAES were observing the hemisphere of interest. MLS ozone is used in the heating rate calculation, except for June 1992, when MLS ozone measurements are not continuously available. Manney et al. (1994c) discuss the impact of using climatological versus MLS ozone. The trajectory code (Manney et al. 1994c) uses a standard fourth-order Runge–Kutta scheme. Winds and temperatures are available once a day and are linearly interpolated to the trajectory time step ($1/2$ h). Heating rates are recalculated every 3 h using interpolated temperatures and are interpolated linearly to the trajectory time step between calculations. Further details are given by Manney et al. (1994c).

Air parcels are initialized on 15 June 1992 and 19 August 1992 in the SH and 3 December 1992 and 14 February 1993 in the NH. The trajectory code was run for 20 days in the June 1992 case, due to the abbreviated observation period, and for 30 days in each of the other cases. The starting dates are chosen a few days after the beginning of the north- or south-looking period, when CLAES data become available for the full day.

b. UARS and UKMO data

The Rossby–Ertel potential vorticity (PV) is also calculated from the UKMO data (Manney and Zurek 1993) and is compared with calculated and observed tracer fields; PV is scaled in "vorticity units" (Dunkerton and Delisi 1986; Manney et al. 1994c) when examining vertical cross sections; this gives a similar range of values for PV on isentropic surfaces throughout the stratosphere.

The CLAES instrument is described by Roche et al. (1993); the CLAES data have a horizontal resolution of ≈400 km and a vertical resolution of ≈2.5 km. The data are still in the validation process; this process has verified that the data used here (v0007) are suitable for studies of morphology and regional variation. Typical single-profile precision and systematic error estimates for N_2O are (20 ppbv rms, 20%) and (10 ppbv rms, 20%) on the 46- and 4.6-hPa surfaces, respectively, and for CH_4 are (100 ppbv, 20%) and (50 ppbv, 20%). In the lower stratosphere, when N_2O (CH_4) mixing ratios exceed ≈210 ppbv (≈1.35 ppmv), values are suspect due to large line-of-sight opacity and the associated lack of tangent point sensitivity (Kumer et al. 1993).

The MLS H_2O data have horizontal resolution of ≈400 km and nominal vertical resolution of ≈4 km, although current retrievals are done at ≈5.5-km vertical resolution. The *UARS* MLS instrument is described by Barath et al. (1993), and the H_2O data by Lahoz et al. (1994). Single-profile precision and accuracy estimates for H_2O are (0.3 ppmv, 15%) at 4.6 hPa (Harwood et al. 1993; Lahoz et al. 1993, 1994). Between ≈20 and 50 hPa, data quality is generally good only at low and middle latitudes. At high latitudes in winter, the data may have a substantial component from climatology at 50 hPa (Lahoz et al. 1994); we thus focus on levels from ≈20 to ≈1 hPa.

Both CLAES and MLS data have been mapped to a 4° latitude by 5° longitude grid; this is consistent with the general meridional resolution of both instruments. CLAES data are gridded by linearly interpolating data for a 24-h period to a regular latitude–longitude grid; ascending and descending orbit tracks are treated separately and then averaged. MLS data are gridded using Fourier transform techniques that separate time and longitude variations (Elson and Froidevaux 1993). Tests using the simple interpolation from 24 h of data for gridding of the MLS data give no significant differences in our results; we therefore believe that this simple gridding used for the CLAES data is adequate for our purposes. All data are interpolated to isentropic (θ) surfaces using UKMO temperatures.

As a preliminary indicator of the utility of the data for the times and analyses done here, gridded passive tracer data have been compared with daily PV fields computed from UKMO data. Since both PV and passive tracers are conserved for adiabatic and frictionless flow, they should show good spatial correlations on individual days, although the relationship between them will change with time due to diabatic effects. Figure 1 shows scatter plots of PV versus N_2O, CH_4, and H_2O at 655 K on 3 December 1992; these are typical of most of the times studied here. Usually, N_2O shows the most compact relationship with PV of the three tracers in the middle and upper stratosphere (above ≈550 K), especially at the high PV values characteristic of the polar vortex region. The correlation of H_2O with PV becomes much weaker at higher levels and high PV values (typical of the polar vortex), especially in the two late winter periods; a compact relationship remains, however, at PV values typical of midlatitudes outside the vortex and along the vortex edge. The correlation between H_2O and PV inside the vortex could be affected by low H_2O descending from the mesosphere, as suggested by Lahoz et al. (1993); in general, however, MLS H_2O shows a mixing ratio peak that, in the polar regions, is located in the middle-to-upper stratosphere throughout the year (Eluszkiewicz et al. 1995). In the lower stratosphere, N_2O usually shows a similar amount of correlation with PV as does CH_4. The exception to this is during the August–September 1992 period, when CH_4 shows a considerably more compact relationship with PV. Additional insight into the usefulness of these data

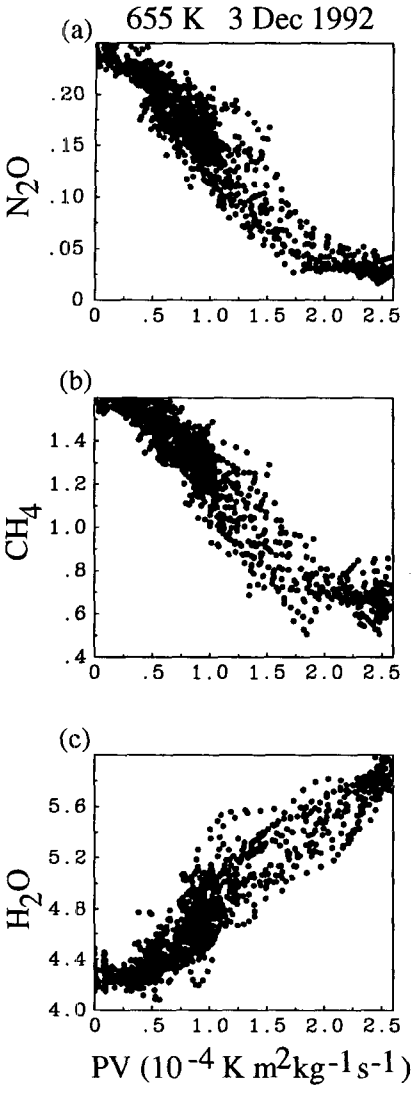

FIG. 1. Scatter plots of potential vorticity (10^{-4} K m^2 kg^{-1} s^{-1}) vs (a) N_2O, (b) CH_4, and (c) H_2O (all in ppmv) at 655 K on 3 Dec. 1992.

will be gained through comparison of results for the different tracers.

c. *Analysis*

Tracer mixing ratios are initially associated with each air parcel by linearly interpolating the gridded *UARS* CLAES or MLS data described above to the 2° latitude by 5° longitude initial parcel grid and to the isentropic surfaces noted above. The evolution of the tracer fields is subsequently predicted by assigning the initial concentration to the location of each parcel at later times, as determined by the forward trajectory calculations. Since these predicted parcel locations will not in general coincide with the points of the observational grid, the predicted fields are compared with observations by interpolating the observed fields to the parcel positions or by gridding the predicted fields at 4° by 5° and on standard isentropic surfaces.

Interpolation of data to predicted parcel positions is straightforward linear interpolation in three dimensions. In addition to comparing observed tracer values at individual parcel positions with those assigned initially to the parcels, the behavior of observed and calculated tracers is compared for ensembles of parcels grouped by their PV and θ values. Differences between calculated and observed average mixing ratios of these ensembles of parcels as a function of PV and θ are most sensitive to gradients in the tracer and PV fields. Figure 2 illustrates this sensitivity, showing as a function of PV and θ the observed N_2O field, the number of parcels in each PV–θ bin [bins are of uniform size in PV and in $\log(\theta)$], and the difference between observed and calculated N_2O fields in each bin, on day 24 (27 December 1992) of the NH early winter simulation discussed here; since N_2O generally has the strongest gradients of the tracers discussed here, it is most sensitive to small errors in parcel positions. Where tracer gradients are strong, a slight error in parcel position leads to a large difference between calculated and observed tracer values. Where PV gradients are strong, fewer parcels are included in each bin (Fig. 2b), making the differences more sensitive to each parcel's position. Thus, the type of diagnostic shown in Fig. 2c indicates where there is the most sensitivity to errors, rather than necessarily showing where the errors are largest. However, strongest tracer gradients are also in regions of strong wind speeds and large wind shears, where errors in calculations of individual parcel positions are expected to be largest (e.g., Morris et al. 1995), so uncertainties in the trajectory calculations are also expected to be larger here. The dipole pattern of differences in Fig. 2c outlines the region where N_2O gradients are strongest (Fig. 2a).

As a measure of differences in the average observed and calculated fields in the vortex region, we will show average, minimum, and maximum observed values at parcel positions for ensembles that group together all parcels initialized at a particular level that are at PV values typical of those inside the polar vortex. Because the number of parcels in this region will change from day to day, the predicted average will change—although each parcel retains the same mixing ratio, the set of parcels averaged over may change from day to day; these changes will be overlaid on the figures. Averages such as this are generally over ≈800–1800 parcels, depending on the hemisphere (because of the larger vortex in the SH) and case being studied. The PV value used to approximately define the vortex, 1.4 × 10^{-4} s^{-1} (in vorticity units), is generally near that where Manney et al. (1994c) showed an abrupt decrease in mixing during the time periods studied here.

Tracer mixing ratios at parcel positions are gridded to the same 4° latitude by 5° longitude grid as the *UARS* data and to "standard" isentropic surfaces from 420

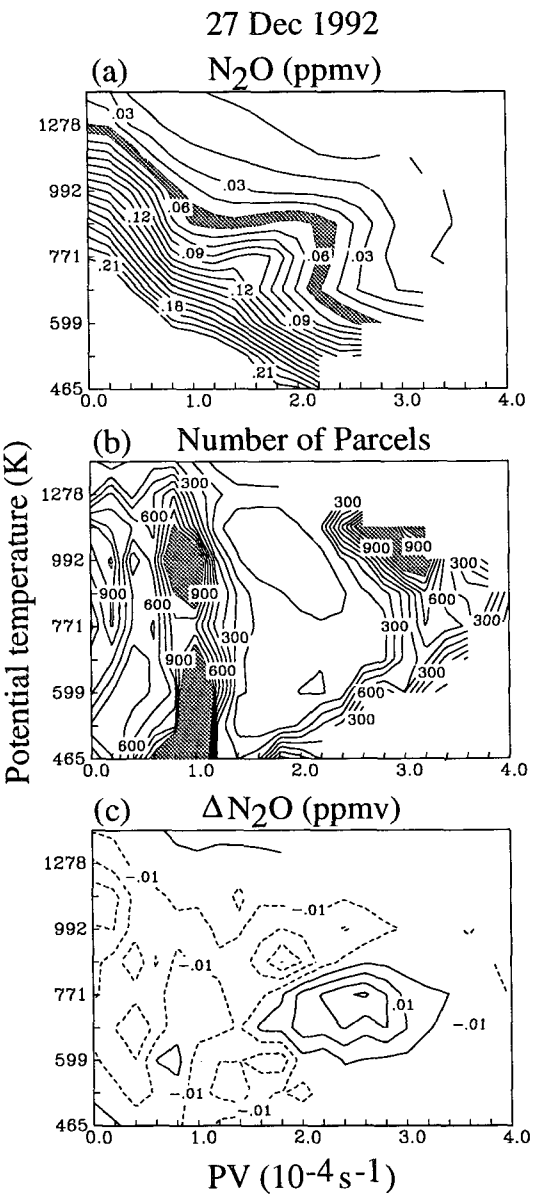

FIG. 2. (a) Observed N_2O as a function of PV and potential temperature (θ) on 27 Dec. 1992; θ runs from 465 to 1450 K; PV is scaled in vorticity units, as described in text, so units are 10^{-4} s^{-1}. (b) Number of parcels from the trajectory run in PV/θ bins centered around the tick marks on 27 Dec 1992. (c) Difference between calculated and observed average N_2O (ppmv) in each of the PV/θ bins shown in (b), calculated as described in text; dashed lines show where calculated values are less than observed values. Blank areas on plots are levels where the corresponding PV value does not exist on that day. Bins are of equal size in scaled PV and in log (θ) and are centered around the tick marks, so they are 0.2×10^{-4} s^{-1} wide in scaled PV and 0.127 wide in log(θ).

through 1700 K that were chosen to be near the *UARS* pressure levels (the levels at which the CLAES data are retrieved); these surfaces are 420, 465, 520, 585, 655, 740, 840, 960, 1100, 1300, 1450, and 1700 K. The gridded fields thus have similar vertical resolution to the CLAES data and have similar horizontal resolution to all the *UARS* data.

Gridding is accomplished by binning the parcels in three-dimensional boxes centered about the final grid points and assigning to each box a mixing ratio equal to the average of the parcels in the box weighted by their normalized three-dimensional distance from the center of the box. Boxes with no parcels are then filled in by linear interpolation, unless many contiguous boxes are missing, in which case those boxes are simply treated as missing data in further analyses. Since no new parcels are added during these simulations, by the end of the runs many areas in approximately the top three levels are not covered.

Several other gridding methods have been tried, as well as gridding at various vertical and horizontal resolutions and initializing at different vertical and horizontal resolutions and on equal area (rather than latitude–longitude) horizontal grids. All of these produced very similar results to the method chosen here. In any gridding that bins and averages a number of points, there are concerns about the appropriate weighting for points originating in different places, that is at much higher or lower latitudes, or much higher or lower altitudes. For example, since the parcels are initialized on a vertical grid that is approximately uniform in altitude, it is appropriate to question whether ignoring the altitude of origin of parcels that end up in a specific bin might bias the mixing ratio toward values characteristic of higher levels. An alternative way of obtaining a gridded field from a Lagrangian trajectory calculation is to use a method similar to that described by Sutton et al. (1994). Parcels are initialized on the 4° by 5° grid used for the *UARS* data on the day that we are interested in examining; the trajectory code is then run backwards in time to the day on which we wish to initialize the tracer mixing ratios. Observed mixing ratios on that initial day are interpolated (using a simple linear interpolation in three dimensions) to the positions of the parcels, and these values are then assigned to the grid point on the later day that we wish to examine. This is very computationally demanding, as it requires doing a separate trajectory calculation for each day for which we calculate the transport. However, the initial parcel mixing ratio is found by a simple linear interpolation from gridded data, and the technique associates a value at a single point on the initialization date with the value at the position that that parcel is calculated to have on the final day. Thus, there is no question about relative weighting of points with different origins.

In the following part of this work (Manney et al. 1995), we use Lagrangian transport calculations to examine the evolution of ozone for the same time periods discussed here. Since ozone has a source in the low-latitude middle stratosphere, we will use there a relaxation to observations to crudely parameterize photochemistry, providing a low-latitude source of ozone, as described in more detail in Manney et al. (1995). It is not feasible to apply this correction when using the

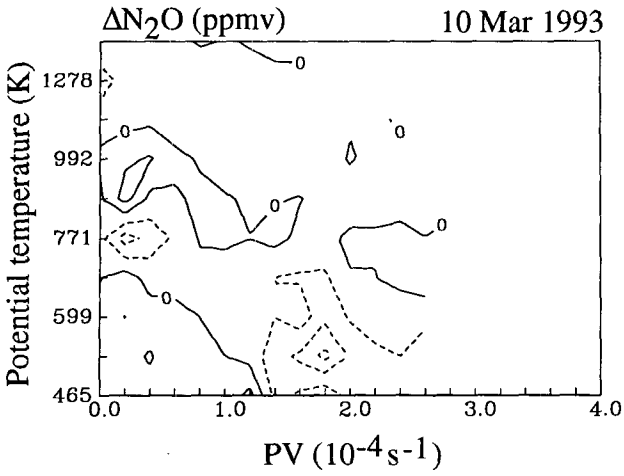

FIG. 3. As in Fig. 2c but with the difference between N_2O values at parcel positions and values from the gridded calculated fields on 10 Mar 1993.

reverse trajectory procedure just described because of additional computational demands. Therefore, except where otherwise noted, the gridded results presented here and in Manney et al. (1995) are obtained using the binning and interpolation procedure. The sensitivity of our results to the gridding procedure is checked using the reverse trajectory calculations. In most cases, there is little difference between the results using the two procedures. The most sensitivity is apparent during the February–March 1993 period in the NH, the most dynamically active period studied here. During this period, noticeable differences are seen in some species and at some levels during the last ≈10 days of the 30 day calculations, as the fields used in the binning and interpolation procedure become more nonuniform. The general nature of the differences (i.e., they do not usually appear to be localized near regions with strong descent) suggests that nonuniformities in both the horizontal and vertical contribute to the disagreement, rather than the dominant factor being an inappropriate weighting of parcels started at different altitudes. We will note in the text cases where there are significant differences between the two procedures.

By using the gridded passive tracer field from the trajectory calculations in place of the observed tracer field in the analyses at parcel positions described above, we can detect some biases that may be present in the gridding procedure—if the gridding were exact, no difference would be seen between the results from the gridded files interpolated back to the parcel positions and the original predicted values at the parcel positions. Figure 3 shows a difference plot similar to Fig. 2c but uses the gridded N_2O field from the calculations in place of the observed N_2O field; we show the late winter NH time period, as it is the most active, and thus we might expect larger errors. As was the case above, the regions where the calculation is most sensitive to errors are highlighted. We can see, though, that the largest biases from gridding on this day are comparable to the precision of the measurements. Figure 4 shows a plot of average, minimum, and maximum values in the vortex region for parcels started at 655 K, as described above, again using the gridded calculated N_2O field in place of the observations; 655 K is chosen as it is a level where the N_2O field is quite sensitive to errors. Differences in this average are very small, suggesting that there is no significant bias caused by the gridding in the polar regions. The gridded field tends to change somewhat less than the parcel field during times of strong wave activity (i.e., around 25 February and 6 March), and extreme values are more moderate, indicating that some degree of smoothing is produced by the gridding. Figures similar to this for other periods and other levels show even smaller differences.

With the gridded passive tracer fields available, the calculations and observations may be compared using any maps, vertical or horizontal sections, or analyses that can be done with the gridded data. In addition to comparing maps of calculated and observed fields, a comparison that is particularly useful in showing whether the calculations reproduce the broad features of the observations is to compare the changes with time in the observed and calculated fields. We will show such comparisons as difference plots between two days (the initial day and a day late in the run) for fields averaged around a PV contour in PV–θ space (e.g., Manney et al. 1994b). We also show vortex averages of observed and calculated results, which elucidate the differences and similarities between average observed and calculated tracer evolution in the vortex.

3. Early winter results

a. Northern Hemisphere, 3 December 1992–2 January 1993

Figure 5 shows the evolution of observed N_2O compared to N_2O values from the trajectory calculation for

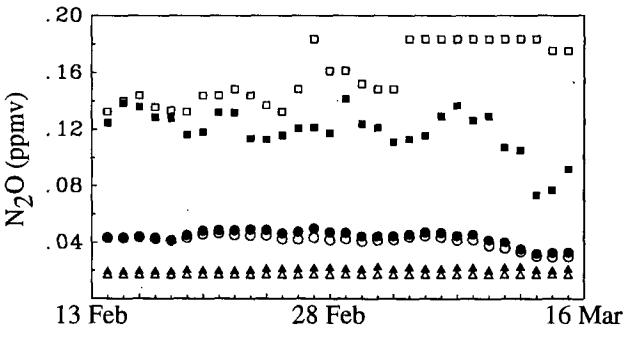

FIG. 4. Average (circles), minimum (triangles), and maximum (squares) N_2O (ppmv) mixing ratios for gridded calculated fields interpolated to the parcels locations (solid symbols) and computed directly from the conserved initial N_2O mixing ratios associated with these parcels (open symbols), for parcels initialized at 655 K that have scaled PV greater than 1.4×10^{-4} s^{-1}, as described in text, for 14 Feb–15 Mar 1993.

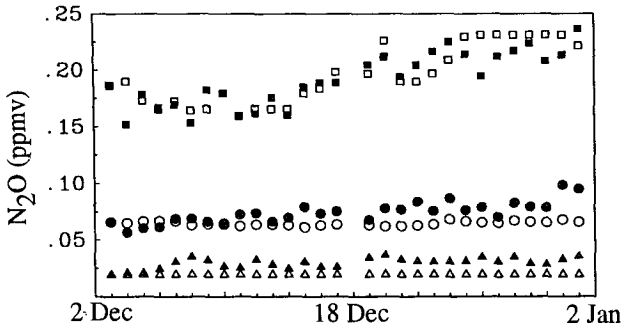

FIG. 5. The average (circles), minimum (triangles), and maximum (squares) values of N_2O mixing ratios (ppmv) as computed by interpolating gridded CLAES observations to the parcel locations determined by trajectory calculations (solid symbols) and as computed directly from the conserved initial N_2O mixing ratios associated with these parcels (open symbols) for 3 Dec 1992–1 Jan 93. The ensemble of air parcels used was initialized at 655 K and is constrained to have a scaled PV $> 1.4 \times 10^{-4}$ s^{-1} on the day considered.

3 December 1992–2 January 1993. The average, minimum, and maximum of observed N_2O values interpolated to the positions of all parcels started on the 655-K isentropic surface that have PV $\geq 1.4 \times 10^{-4}$ s^{-1} (an approximate definition of the polar vortex edge) on each day are shown. Because the number of parcels meeting this condition changes somewhat from day to day, the average, minimum, and maximum for the calculated fields may change as different parcels are included in the average; these values are shown as open symbols. In general, differences between the two curves are small, indicating that observed and calculated fields behave similarly within the polar vortex. Since N_2O decreases with increasing altitude and with increasing PV, the small increase of the observed values with respect to the calculated ones could suggest that the calculated diabatic descent is too strong or that the calculated transport into the vortex is too weak. The fact that maximum values increase similarly both for calculations and observations suggests that the transport toward higher PV is captured by the trajectory calculations. Consistent results are seen for H_2O and CH_4 (not shown).

Figure 6 shows the pattern of N_2O mixing ratios for parcels initialized at 840 K, on day 16 (19 December 1992) of the run, and the mixing ratios from CLAES data interpolated to those parcel positions. As shown by Manney et al. (1994c), most of these parcels are descending during the period. The large-scale features of the observed fields, particularly shape and movement of the polar vortex, are reproduced in the predicted fields. Although on this day regions of high mixing ratios in midlatitudes over the eastern Pacific Ocean and over eastern Europe and Asia can still be seen in the calculated fields (Fig. 6b), by the end of the run a large degree of mixing is seen of parcels with high and low mixing ratios in midlatitudes. After day 16 most distinct midlatitude features are washed out in the trajectory calculations. Figure 6 shows that, although the calculated features are somewhat "mixed up," comparable amounts of high N_2O are drawn up from low latitudes in the calculations and the observations. The presence of higher values along the inside of the vortex-edge region in the calculated field suggests that transport into the vortex region may in fact be slightly stronger in the calculations than in the observations.

Figure 7 shows synoptic maps of N_2O and H_2O from the trajectory calculation and from observations at 655 K on day 8 (11 December 1992); PV contours in the region of strong PV gradients are overlaid on the observed fields to indicate the position and extent of the polar vortex. At this point in the run, agreement is very good within the polar vortex for both tracers, and distinct midlatitude features corresponding to observations are still seen in the calculated fields, showing comparable amounts of high N_2O and/or low H_2O drawn up from low latitudes in calculations and observations.

In Figure 2a, we showed the observed N_2O field on day 24 (27 December 1992) of this run as a function of PV and θ. Figure 8 shows the corresponding calculated N_2O field for this day and differences between this day and the initial day for observed and calculated N_2O. This is during an early winter minor stratospheric warming, when N_2O within the vortex increased over a wide range of levels, as will be seen below. In both observed and calculated N_2O fields there is a steepening of gradients inside the vortex edge and at low PV values, forming a pattern of decreases in N_2O at low PV and increases along the edge of the vortex. This results from air being drawn up from low latitudes around the vortex, which serves to steepen tracer gradients along the vortex edge—this is the formation of the main-vortex/surf-zone structure (e.g., McIntyre and Palmer

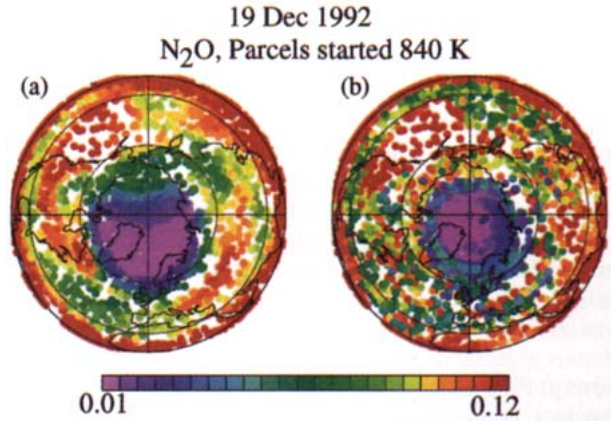

FIG. 6. (a) Observed and (b) predicted N_2O (ppmv) at positions of parcels started at 840 K on day 16 (19 Dec 1992) of the run started 3 Dec 1992. Predicted values are the values at the parcel positions on the initial day, advected with the parcels. Observed values are interpolated to the parcel positions from the gridded *UARS* CLAES data on each day. Most of the parcels shown are moving downward during the run (Manney et al. 1994c).

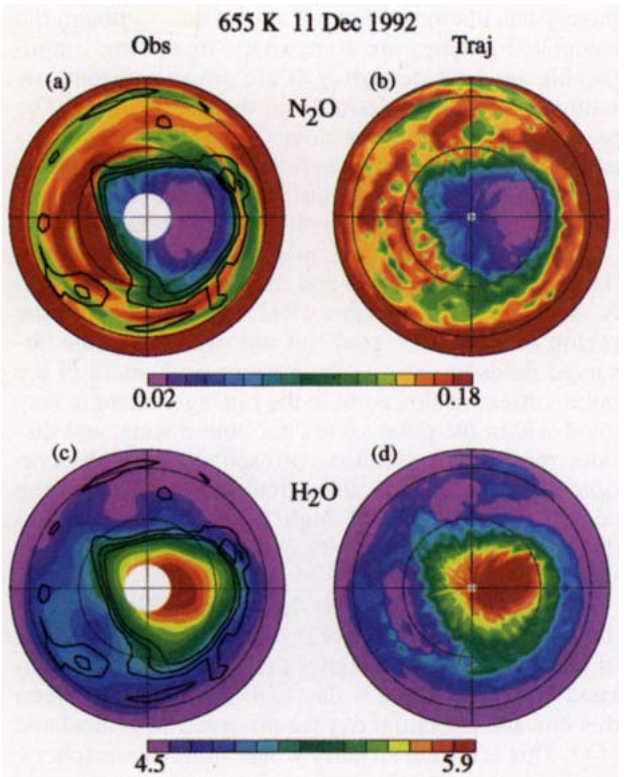

FIG. 7. Synoptic maps of N_2O (ppmv) and H_2O (ppmv) mixing ratios from observations (a and c) and from the trajectory calculation (b and d) started on 3 Dec 1992, on day 8 (11 Dec 1992) of the calculation at 655 K; PV contours in the region of strong gradients are superimposed on the observed fields; these contours are 1.0, 1.2, and 1.4 $\times$ 10^{-4} K m^2 kg^{-1} s^{-1}. The projection is orthographic, with 0° longitude at the bottom of the plot and 90°E to the right; dashed lines show 30° and 60° latitude circles.

1984). The dipole pattern of increases along (and inside) the vortex edge and decreases outside the edge, which appears in both observations and calculations, indicates that these horizontal transport and mixing processes are dominating over diabatic descent in changing the N_2O field at this time. Both the increase and decrease are weaker in the predicted fields than in the observations. There are regions of slight decrease in the polar upper and lower stratosphere, where descent apparently dominates in the calculations. In a complex situation such as this, it is difficult to determine whether in fact the diabatic descent is too strong or the poleward transport is too weak. A very similar pattern is seen in CH_4. The fact that there is good qualitative agreement in the calculated and observed patterns at PV values well outside the vortex indicates that the lack of detailed agreement at midlatitudes is due mainly to random errors and/or small-scale effects that, when averaged in this way, give the correct type of large-scale behavior in midlatitudes. Differences between observed and calculated fields at the lowest PV values shown indicate the failure of the trajectory calculations to reproduce the strong subtropical tracer gradients seen in observations. While the exact cause of this failure in the trajectory calculation is not obvious, the low latitudes are generally regions where we have less confidence in the details of the wind fields that are used.

Figure 9 shows observed and calculated H_2O on day 24 and the difference of each from the initial (day 0) field. MLS H_2O measurements in the polar regions show mixing ratios peaking in the upper stratosphere ($\approx$1000–1400 K) throughout the year (Eluszkiewicz et al. 1995). At levels below this peak, it is expected that H_2O mixing ratios will increase (decrease) where N_2O and CH_4 mixing ratios decrease (increase). Above

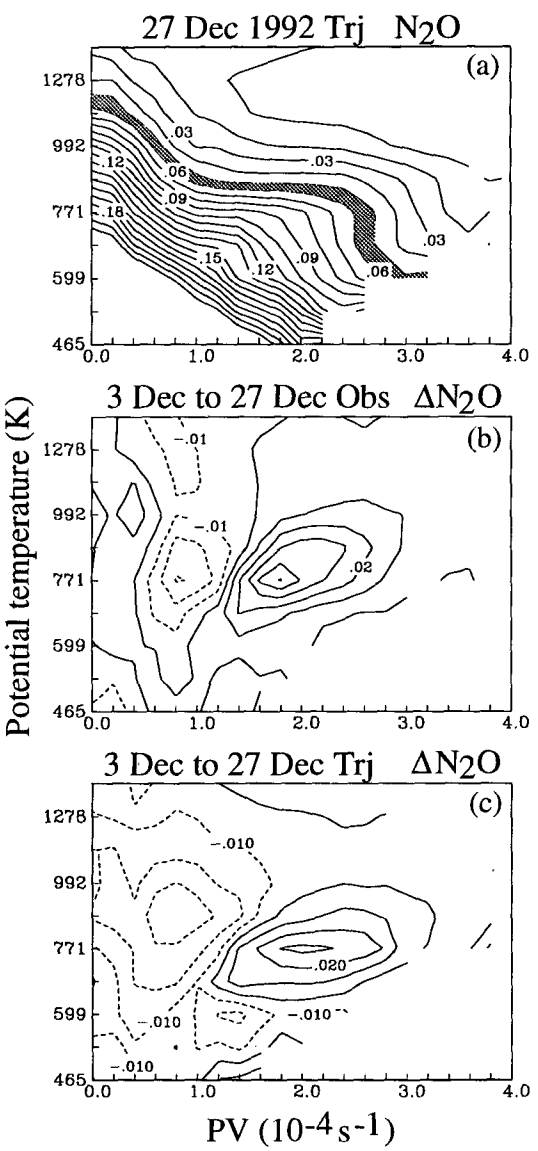

FIG. 8. (a) As in Fig. 2a but showing calculated N_2O mixing ratio (ppmv) as a function of PV and θ on 27 Dec 1992; (b) and (c) differences (ppmv) in (b) observed and (c) calculated N_2O fields between 3 Dec and 27 Dec 1992, as a function of PV and θ; dashed lines indicate a decrease over the time period.

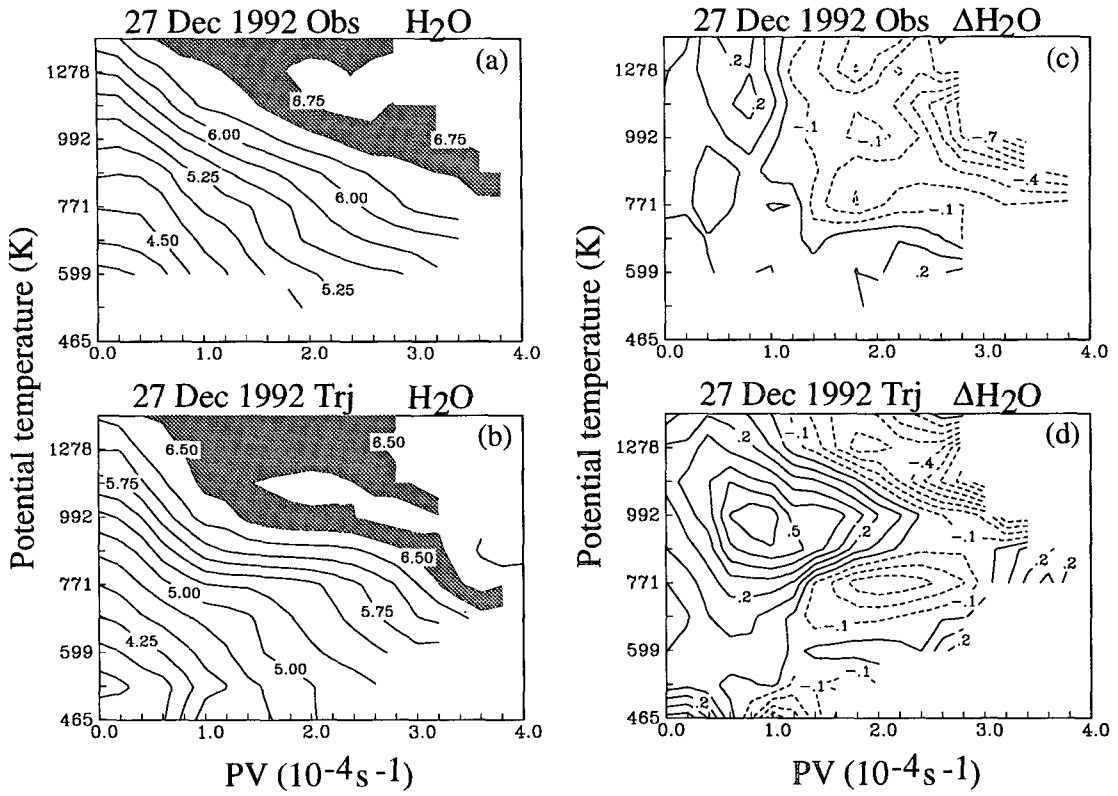

FIG. 9. (a) Observed and (b) calculated H_2O mixing ratios (ppmv) as a function of PV and θ on 27 Dec 1992; (c) and (d) differences (ppmv) in (c) observed and (d) calculated H_2O mixing ratios (ppmv) between 3 Dec and 27 Dec 1992; dashed lines indicate a decrease over the time period. The blank space at the bottom of the plots from observations shows the levels at which H_2O data are considered unreliable.

the level of the peak, the downward motion would cause H_2O mixing ratios to decrease; horizontal transport toward the vortex center would generally decrease H_2O, except when, as is sometimes the case in the upper stratosphere (e.g., Lahoz et al. 1994), the maximum H_2O mixing ratios do not extend to the center of the vortex. The pattern expected from this behavior is shown in Fig. 9d (the calculated differences), where there is a dipole pattern opposite to that for N_2O in the midstratosphere and decreases in the polar upper stratosphere. Figure 9c shows H_2O mixing ratios decreasing at all levels above $\approx$650 K and PV values greater than $\approx 1.0 \times 10^{-4}$ s^{-1}. [This is outside the vortex edge; Manney et al. (1994c).] Since MLS H_2O measurements indicate a relatively shallow peak in H_2O mixing ratios in the upper stratosphere (e.g., Fig. 9a), it is likely that the current H_2O retrievals may miss the peak on some days, giving the appearance of a decrease in H_2O mixing ratios. The differences between the behavior of H_2O and other tracers, and between calculated and observed H_2O fields, suggest some possible inconsistencies in the observed fields within the polar vortex in the middle and upper stratosphere.

To obtain information on average descent rates in the vortex, we examine time series of vortex-averaged tracers for the lower (420–655 K) and middle stratosphere (655–1300 K); Figure 10 shows these for N_2O. Since horizontal transport across the vortex edge is limited, descent should be a significant factor in changing these averages; we have already seen that in this case it is not the only, or even the dominant, factor in the middle stratosphere. Most major features in the observations are reproduced in the calculations, for instance, temporary increases in N_2O near $\approx$650–800 K around 7, 15, and 24 December 1992. These increases occur at times of particularly strong wave activity and are probably due to large tongues of high N_2O being drawn up around the vortex from low latitudes; some of these higher values are probably included in the average shown here. Although horizontal transport plays an important role in the evolution shown here, especially in the midstratosphere, Figs. 5–7 suggested good agreement between the large-scale horizontal motions in observations and calculations in the midstratosphere. With this in mind, the overall trends suggest that the calculated descent rates are too strong during December 1992 in the NH middle stratosphere. Assuming all of the net change in the contours over the period is due to vertical motions, a rough estimate from the data would suggest a diabatic descent rate ($d\theta/dt$) at $\approx$900 K of ≈ -1.3 K/d; the calculated fields suggest ≈ -2 K/d. In the lower stratosphere, rough estimates from

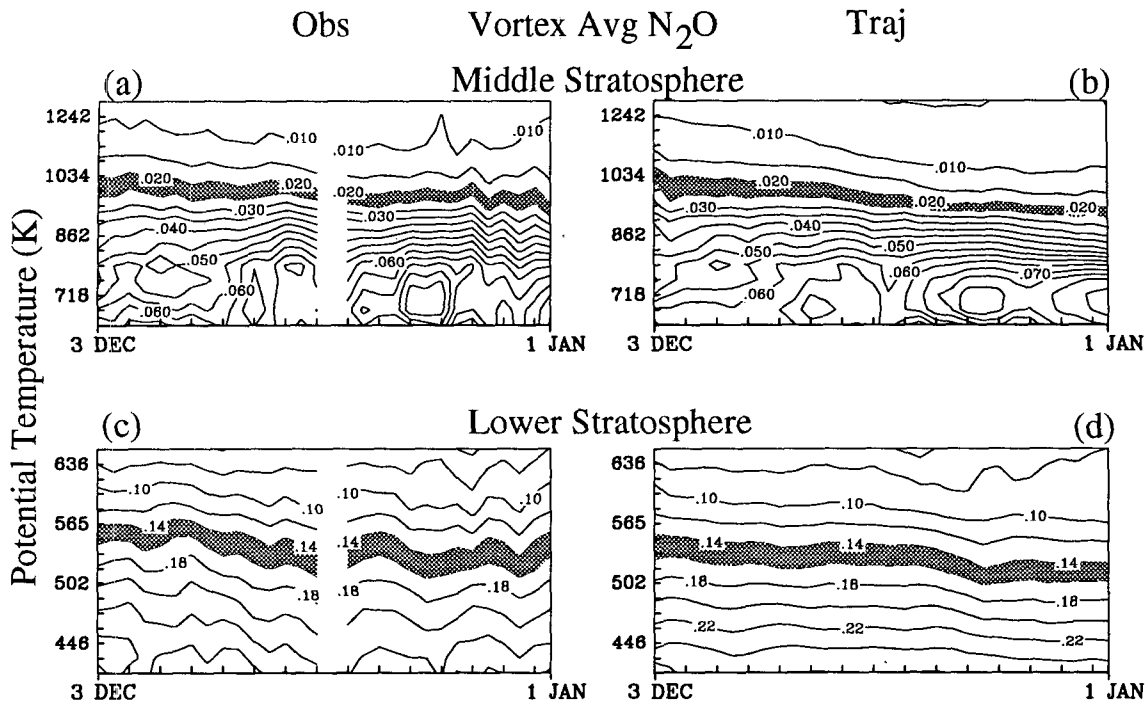

FIG. 10. Time series of vortex-averaged N_2O mixing ratios (ppmv) as a function of θ in the midstratosphere (655–1300 K) (a and b) and lower stratosphere (420–655 K) (c and d) for 3 Dec 1992–1 Jan 1993. Vortex averages are area weighted and are computed using the 1.4×10^{-4} s^{-1} scaled PV contour as an approximate definition of the vortex edge. Values between 0.02 and 0.025 ppmv are shaded in the middle stratosphere plots and between 0.14 and 0.16 ppmv in the lower stratosphere plots. Observed fields are on the left; calculated fields on the right.

observations and data suggest a diabatic descent rate of from ≈ -0.9 to -1.0 K/d at ≈ 550 K.

b. *Southern Hemisphere, 15 June–5 July 1992*

Figure 11 shows a time series, similar to that in Fig. 5, for 15 June–5 July 1992 of the average, minimum, and maximum of observed and calculated N_2O values interpolated to the positions of all parcels started on the 655-K isentropic surface that have $|PV| \geq 1.4 \times 10^{-4}$ s^{-1} on each day. Since horizontal transport across the vortex edge is extremely limited during this period (Manney et al. 1994c), we expect changes here to be dominated by diabatic effects. Differences between the two average curves are small, but in this case observed values decrease with respect to calculated values, suggesting that diabatic descent rates may be too weak. Similar results are seen for CH_4.

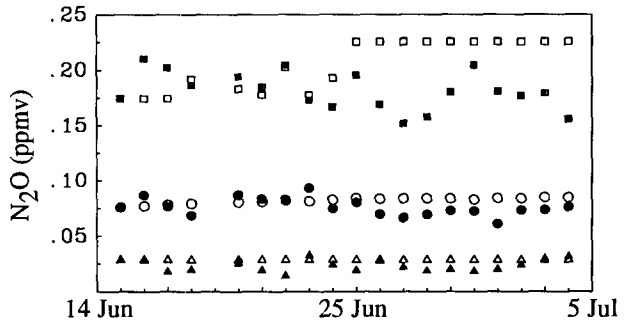

FIG. 11. As in Fig. 5 but for 15 Jun–4 Jul 1992 in the SH for parcels started at 655 K with |PV| greater than 1.4×10^{-4} s^{-1}.

The polar vortex is quite symmetric during this period, and maps comparing observed and calculated tracer values (not shown) indicate general agreement in the size and shape of the vortex and, as in the NH case discussed above, considerable mixing in midlatitudes of parcels with high and low mixing ratios.

Figure 12 shows difference plots in PV–θ space for observed and calculated N_2O between day 20 (5 July 1992) and day 0 (15 June 1992) of the run. The observed plot shows large decreases in N_2O throughout most of the domain, suggesting that diabatic descent is dominating. The calculated fields shows much smaller decreases over most of the domain, with reasonable agreement between the two only in the lower stratosphere (below ≈ 700 K) well inside the vortex ($|PV| > \approx 2.4 \times 10^{-4}$ s^{-1}).

Figure 13 shows vortex-averaged N_2O for lower and middle stratosphere regions. In the middle stratosphere, the general variations in the contours are reproduced by the calculations but with significantly less descent of the contours in the calculated field. The lower stratospheric calculations also suggest less descent, with an

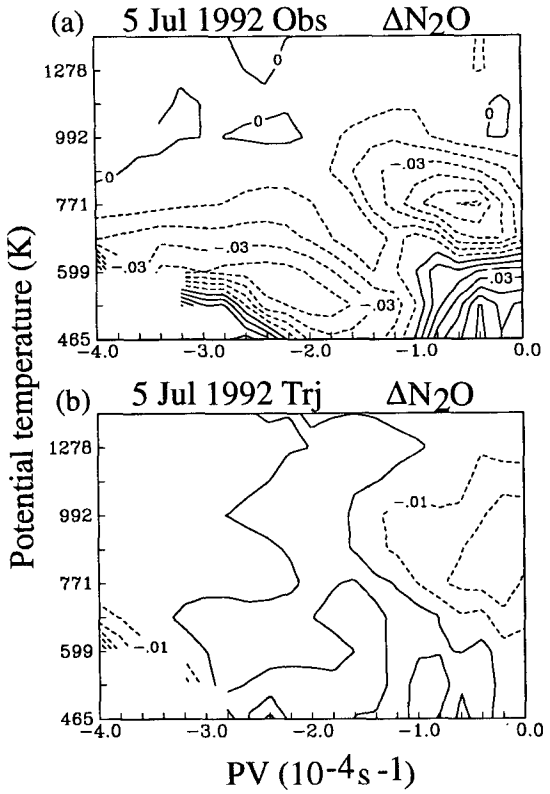

FIG. 12. As in Figs. 8b and 8c but for 5 Jul 1992 with calculated values from run started 15 Jun 1992. Note |PV| increases to the left in the SH plots.

estimate of diabatic descent at ≈550 K of ≈−0.3 K/d from the calculations but near −1 K/d from observations. When these area averages are done for a more restricted region in the center of the vortex ($|PV| > 2.2 \times 10^{-4}$ s^{-1}), agreement is somewhat better, with ≈−0.9 K/d diabatic descent from the calculations and ≈−1.1 K/d from observations. The calculations, therefore, do not show strong descent over as large a region as the observations. The differences between observations and calculations shown here point to a significant underestimate of diabatic descent in the radiation calculation used. Since for these cases that calculation depends most strongly on temperature, the differences also suggest a possible bias in the SH UKMO temperatures at this time.

4. Late winter results

a. Northern Hemisphere, 14 February–16 March 1993

Figure 14 shows a time series for 14 February through 16 March 1993 of the average, minimum, and maximum of observed and calculated N_2O and CH_4 values interpolated to the positions of all parcels started on the 655-K and 465-K isentropic surfaces that have $PV \geq 1.4 \times 10^{-4}$ s^{-1} on each day. At 655 K, the calculated values diverge temporarily from the observed values during a strong stratospheric warming in late February (Manney et al. 1994a) and again move away from observed values in the last few days of the run, during another strong warming. During these warmings, large tongues of low-latitude air are drawn up around the vortex, and air is drawn off the vortex into low latitudes. During the latter warming, the area enclosed by the region of strong PV gradients decreases, and the strong gradients move to higher PV values; a large increase is seen in horizontal mixing (Manney et al. 1994c), indicating a weaker barrier to transport. Thus, changes in these averages are not dominated by vertical motions. The increase in observed values with respect to calculated values could indicate either that the trajectory model predicts less transport of low-latitude air into the vortex region (or more transport of vortex air toward lower latitudes) or that the radiation calculation predicts diabatic descent that is too strong in the polar midstratosphere. Consistent results are seen at 840 K and for H_2O at 655 K; at 840 K observed H_2O values decrease with respect to calculated values throughout the period.

At 465 K, in the lower stratosphere, although the observed values show some scatter about the calculated values, there is no apparent trend in the difference between the two, and observed and calculated values remain close throughout the period. Average CH_4 values here are very close to those above which the data become suspect and thus may be less reliable.

Figure 15 shows maps of N_2O mixing ratios at the locations of parcels started at 655 and 840 K, on day 24 (10 March 1993) of the run. We see general agreement in the shape and position of the low N_2O values that identify the polar vortex. As in the early winter cases, calculated extravortex values show parcels with high and low mixing ratios in close proximity. This results, at least partly, from the lack of any parameterization of mixing in these calculations. Larger errors in the trajectory calculations are also expected in the region of strong wind shear just outside the vortex (e.g., Morris et al. 1995).

At 655 K, a narrow tongue of low N_2O mixing ratios is drawn off the edge of the vortex along 270°–360°E, near 30° latitude. This feature does not appear in the observations but could be sufficiently narrow and located so as to be missed by *UARS* (e.g., Morris et al. 1995); similar features have been seen in very high-resolution simulations of Arctic vortex evolution (e.g., Waugh et al. 1994). At 840 K, the position, size, and mixing ratios in the blob of high N_2O drawn into the anticyclone are comparable in observations and calculations, although the gradients about its edges are sharper in the calculations. This is expected since the lack of a small-scale mixing parameterization leads to stronger gradients in the calculations, and the low resolution leads to weaker gradients in the observations. Detailed agreement in midlatitudes, outside the vortex, is poor at 655 K, as in the previous cases discussed. A

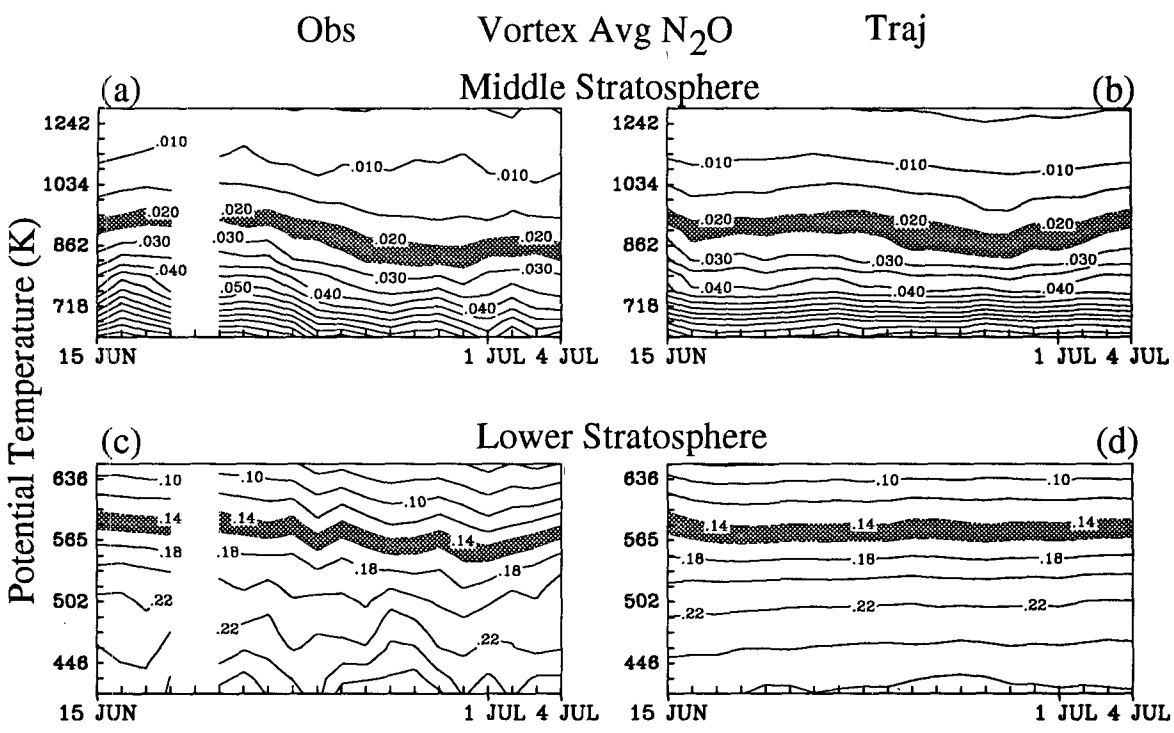

FIG. 13. As in Fig. 10 but for 15 Jun–5 Jul 1992 in the SH using |PV| greater than 1.4×10^{-4} s^{-1} to approximately define the vortex edge.

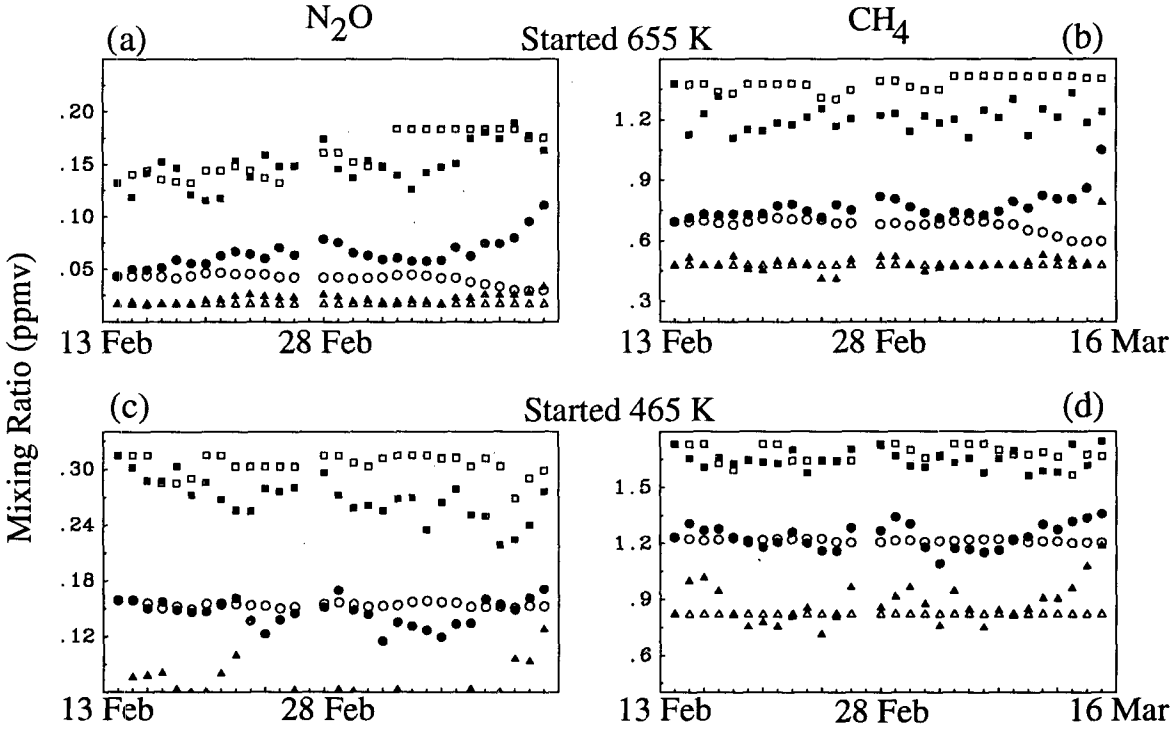

FIG. 14. As in Fig. 5 but for both N_2O (a and c) and CH_4 (b and d) and for parcels started both at 655 (a and b) and 465 K (c and d) for 14 Feb–15 Mar 1993 in the NH.

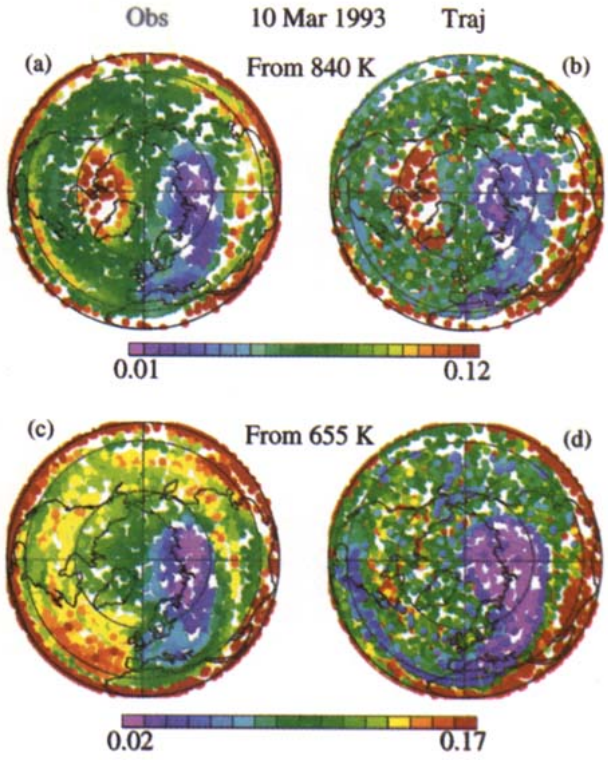

FIG. 15. As in Fig. 6 but for parcels started at 840 (a and b) and 655 K (c and d) on 14 Feb 1993, plotted on day 24 of the run (10 Mar 1993); (a) and (c) show observed fields, and (b) and (d) show calculated fields.

narrow line of high N_2O is seen at 840 K over the southern United States; in this instance a similar feature is apparent in the observations. Figure 16 shows synoptic maps of N_2O at 840 K on day 16 (2 March 1993) from observations and gridded calculations. Again, good agreement is seen between observed and calculated N_2O values, both within the vortex and in the region of the anticyclone. As expected, stronger gradients are seen at the edges of both regions in the calculations.

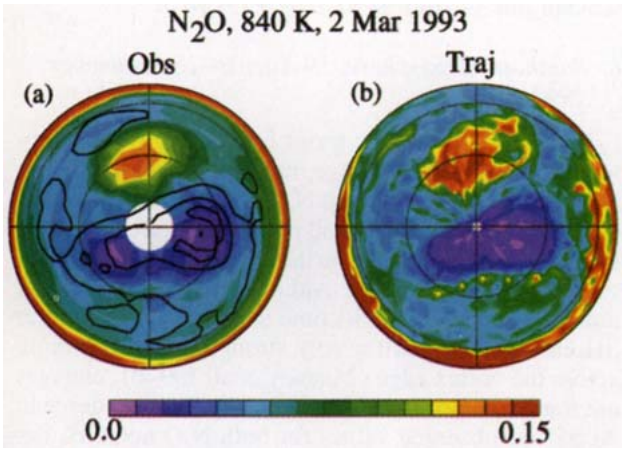

FIG. 16. As in Fig. 7 but for N_2O mixing ratios (ppmv) at 840 K on day 16 (2 Mar 1993) of the run started on 14 Feb 1993. The overlaid PV contours at 840 K are 3, 5, and 7×10^{-4} K m^2 kg^{-1} s^{-1}.

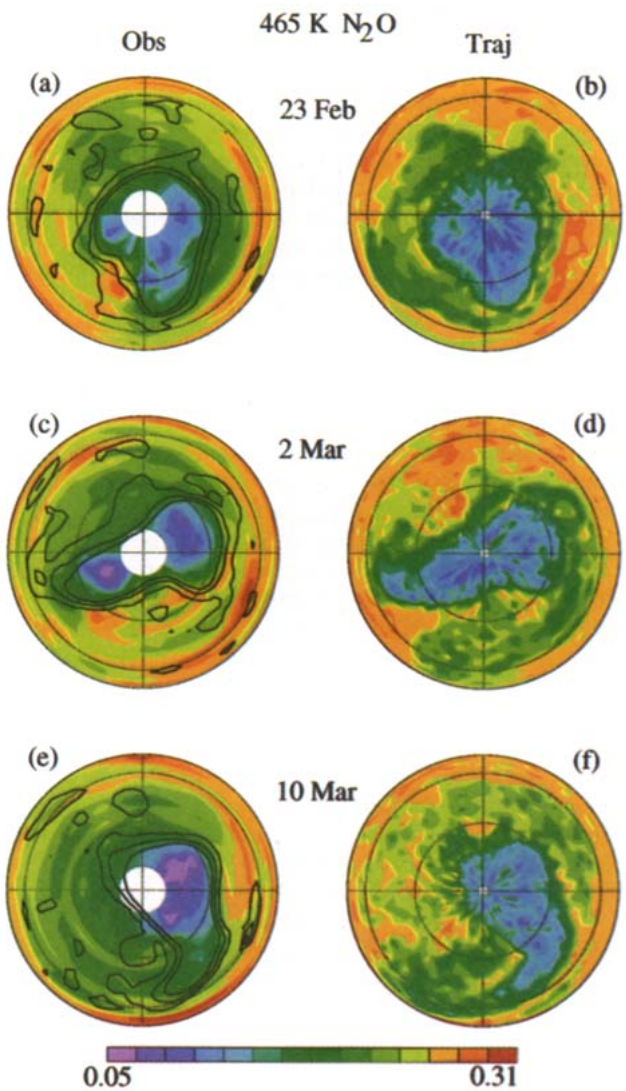

FIG. 17. As in Fig. 16 but at 465 K, on days 8 (22 Feb 1993), 16 (2 Mar 1993), and 24 (10 Mar 1993). The overlaid PV contours at 465 K are 0.2, 0.25, and 0.3×10^{-4} K m^2 kg^{-1} s^{-1}.

Figure 17 shows synoptic maps of N_2O at 465 K on days 8 (23 February), 16 (2 March), and 24 (10 March). We restrict our attention mainly to the vortex region, since N_2O (and CH_4) mixing ratios outside are generally higher than we have confidence in; however, some features outside the vortex, for example, a tail coming off the vortex edge near 45°E on 2 March and one near 0° longitude on 10 March, appear to be related to features in the calculated fields and in the PV field. There is generally good agreement between the size and shape of the region of low N_2O and the vortex as defined by PV and, consequently, a strong correspon-

dence between the observed and calculated low N_2O regions. Minimum N_2O values are slightly higher in the calculations on day 24 (10 March).

Figure 18 shows difference plots in PV–θ space between N_2O on day 24 (10 March) and day 0 (14 February) of the run in observations and calculations. The patterns shown agree well below ≈800 K but with somewhat larger decreases in observations between ≈500 and 650 K near the vortex edge. Agreement is not as good in the upper stratosphere; however, the N_2O values are much lower here, and the changes over this time period smaller. Slightly better agreement was obtained here using the reverse trajectory procedure described in section 2c; however, the differences between the two methods of obtaining gridded fields and the actual differences with time are of the same approximate magnitude as the precision of the data. Increases in observations in the upper stratosphere suggest horizontal transport toward higher PV, up to the highest PV values present; the more-restricted region of increase in the calculations suggests that horizontal transport at very high PV may be underestimated or that diabatic descent may be overestimated in the same region. The differences at low PV values show, as was the case in the NH early winter, that the calculations fail to reproduce sufficiently strong subtropical tracer gradients.

Figure 19 shows the distribution of H_2O in PV–θ space on the initial day (14 February 1993), the observed and calculated distributions on day 24 (10 March), and the corresponding difference plots for observations and calculations. As was mentioned in the NH early winter case, an apparent nonconservation of H_2O is seen in the polar upper stratosphere in observations, possibly related to the coarse vertical resolution of the current MLS retrievals. This is not an artifact of the averaging around PV contours, as it also appears when individual vertical sections are examined. As a result of this, Figs. 19d and 19e show poor agreement between observations and calculations in the polar upper stratosphere. The calculated fields show behavior consistent with that of N_2O and CH_4, while the observed fields show decreases in H_2O over a larger region than would be expected. The reverse trajectory procedure for obtaining a gridded field gave a maximum increase in H_2O over this period between ≈800 and 1000 K of only about 2/3 of that shown in Fig. 19e. However, the qualitative pattern was similar and quantitative agreement was good in other regions. Thus, although there is some uncertainty introduced by the gridding, there remains a distinct qualitative difference between observed and calculated H_2O fields.

Figure 20 shows vortex-averaged N_2O in the lower and middle stratosphere. In the middle stratosphere, both observations and calculations show increases in N_2O, which result from the increase in horizontal mixing at high PV values at this time (Manney et al. 1994c). The increases are considerably larger in the observations, consistent with the differences shown in Fig. 18. Since Figs. 15 and 16 suggest that the large-

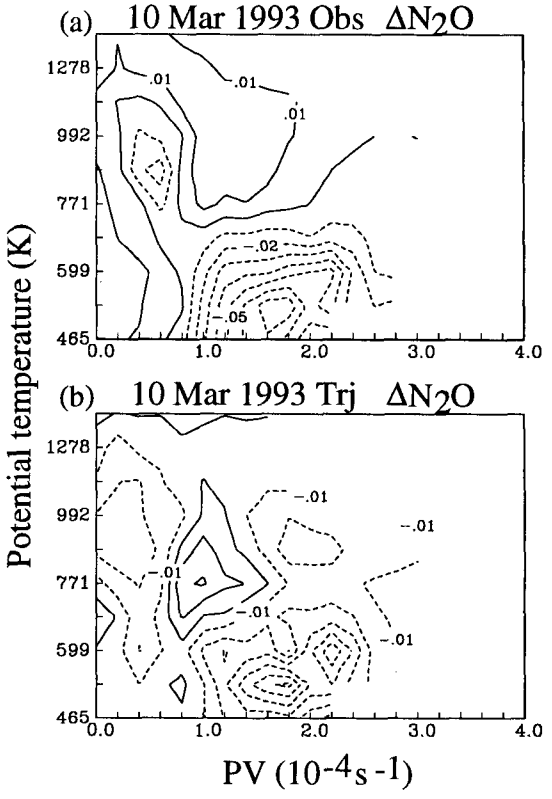

FIG. 18. As in Figs. 8b and 8c but on 10 Mar 1993 from run started on 14 Feb 1993.

scale horizontal transport is reproduced by the calculations, these differences indicate that diabatic descent may be too strong in the midstratosphere. Below ≈840 K, temporary increases around 26 February and 8 March, near the peaks of the two warmings (Manney et al. 1994a), are also apparent in the calculations. In the lower stratosphere, rough estimates of descent rates at ≈500–550 K are comparable for observations and calculations during the first 27 days, giving a diabatic descent rate of from ≈−1.0 to −1.4 K/d.

b. Southern Hemisphere, 19 August–18 September 1992

Figure 21 shows time series for 19 August–17 September 1993 of the average, minimum, and maximum of observed and calculated N_2O and CH_4 values interpolated to the positions of all parcels started on the 655-K and 465-K isentropic surfaces that have $|PV| \geq 1.4 \times 10^{-4}$ s^{-1} on each day. Although there is somewhat more wave activity at this time than in the early winter SH case, there is still a very strong barrier to mixing across the vortex edge (Manney et al. 1994c); changes are thus expected to be dominated by diabatic descent. At 655 K, observed values for both N_2O and CH_4 decrease with respect to calculations, suggesting that calculated diabatic descent is not strong enough at this level. At 465 K, while CH_4 observations show little

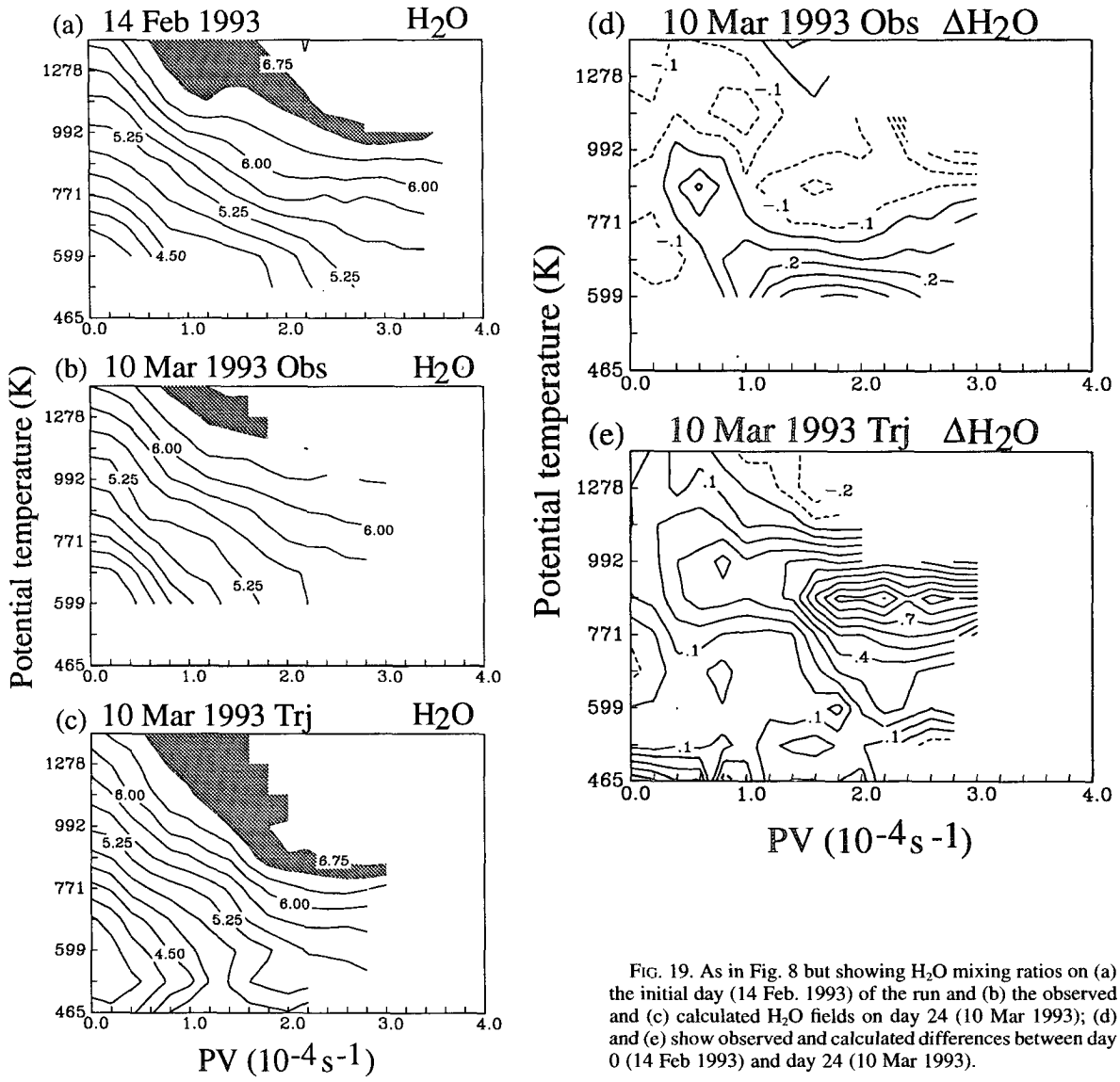

FIG. 19. As in Fig. 8 but showing H_2O mixing ratios on (a) the initial day (14 Feb. 1993) of the run and (b) the observed and (c) calculated H_2O fields on day 24 (10 Mar 1993); (d) and (e) show observed and calculated differences between day 0 (14 Feb 1993) and day 24 (10 Mar 1993).

overall trend with respect to calculations, the observed N_2O values show a sudden decrease over a few days around 1 September 1992. The average N_2O values before 1 September 1992 are at or in some cases slightly above that (>210 ppbv), above which N_2O values become suspect. It appears, therefore, that CH_4 may be somewhat more reliable than N_2O in the lower stratosphere during this period; as noted above, CH_4 shows a stronger correlation with PV than N_2O in the lower stratosphere during this period.

Figure 22 shows a plot similar to Fig. 21 but for H_2O at 840 K. Behavior consistent with that of N_2O and CH_4 would lead us to expect that observed H_2O values would increase with respect to calculations, since 840 K is below the H_2O mixing ratio peak at this time. In contrast to this expectation, observed H_2O decreases steadily with respect to calculations. Examination of vertical sections for this period shows, as in other periods, decreases in maximum H_2O mixing ratios at high latitudes. Again, we see evidence that the current MLS H_2O fields in the polar upper stratosphere exhibit behavior inconsistent with that expected for a passive tracer inside the polar vortex.

Synoptic maps of N_2O and CH_4 in the middle stratosphere show good agreement between the large-scale evolution of observed and calculated fields, as was seen in the other cases, and H_2O maps show good agreement along and outside the vortex edge. Figure 23 shows maps of observed and calculated CH_4 at 465 K on day 24 (12 September) of the run. As was the case in the late winter NH, there is good agreement between the shape, size, and position of the vortex, and mixing ratios are similar in both cases.

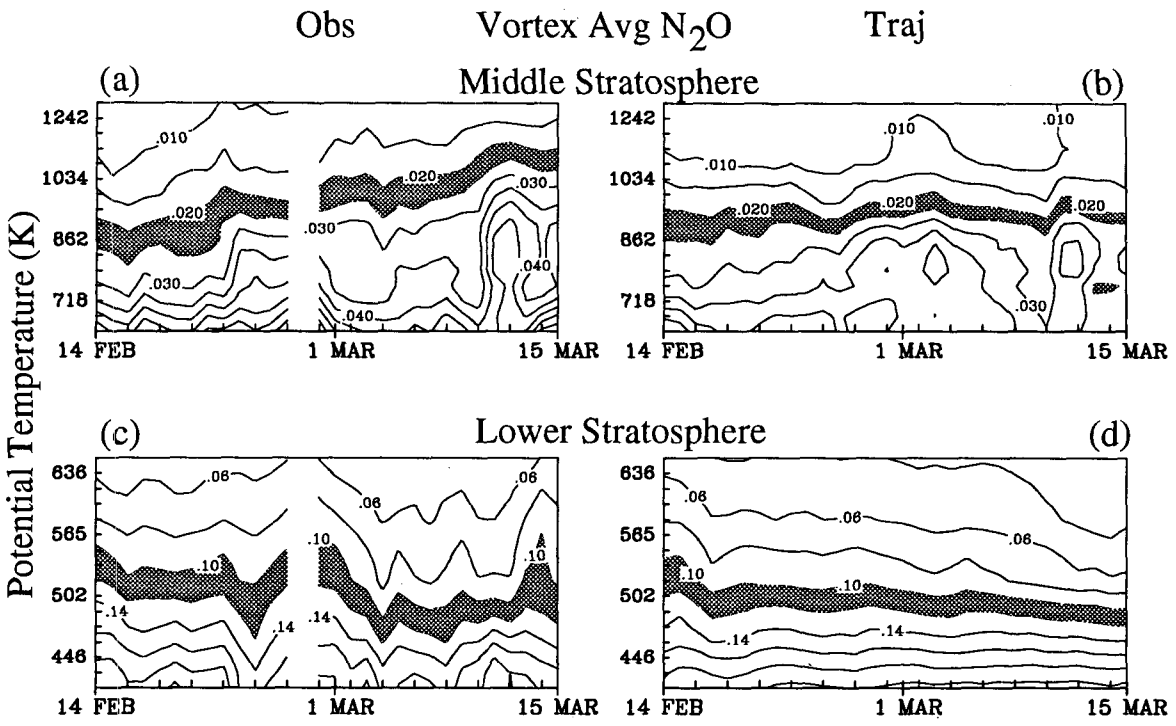

Figure 24 shows difference plots in PV–θ space for N_2O and CH_4 between day 24 (12 September) and day 0 (19 August) in observations and calculations. The N_2O plots show good agreement, except in the lower stratosphere, where the observations show a much larger decrease near the pole and a decrease extending further out toward the vortex edge. The CH_4 plots agree much better in the polar lower stratosphere. Both N_2O and CH_4 show a larger increase at $\approx$800 K in the calculations than in the observations; if the calculated diabatic descent is in fact too weak, the effects of poleward transport would be more pronounced in the calculated changes. Very similar results for N_2O and CH_4 were obtained using the reverse trajectory procedure.

In the late winter SH middle stratosphere, N_2O and CH_4 have very weak gradients inside the vortex; vortex averages therefore give little information about their transport; middle stratospheric vortex averages for H_2O show the same apparent nonconservation that was demonstrated by Fig. 22. Figure 25 shows vortex-averaged N_2O and CH_4 in the lower stratosphere. The contours in the calculated plots are nearly flat, suggesting little or no diabatic descent or, in the case of CH_4, slight ascent. Both N_2O and CH_4 observations show a discontinuity around 1 September 1992. If estimated separately for the periods before and after this, the observations also show little or no descent and, for CH_4 in the latter half of the period, slight ascent. Figures 24c and 24d showed that CH_4 decreased in the lowest levels for $\approx 1.4 \times 10^{-4}\ s^{-1} \leq |PV| \leq 2.4 \times 10^{-4}\ s^{-1}$ but increased at higher |PV|. When an average similar to that shown in Fig. 25 is done for the 1.4–2.4 $\times 10^{-4}\ s^{-1}$ |PV| band, the descent rate at $\approx$500–550 K is estimated to be ≈ -0.3 K/d from both calculations and CH_4 observations. These estimates, and the results shown by Manney et al. (1994c), indicate that in this SH late winter significant descent in the lower stratosphere is confined to a ring along the vortex edge. As was the case in the SH early winter, calculations appear to show a more limited region of descent in the lower stratosphere than observations.

5. Summary

Trajectory calculations in which air parcels are initialized on a three-dimensional grid filling the stratosphere in one hemisphere are used to examine transport by assigning to each parcel the observed mixing ratio of an atmospheric trace species on the initial day and then tracking the parcel locations on subsequent days. This technique is applied to passive tracer data, namely N_2O and CH_4 from CLAES and H_2O from MLS. Four periods when the two *UARS* instruments were viewing high latitudes during early and late winter in the NH and in the SH are examined.

In general, the average characteristics of the calculated fields agree well with observations inside the polar vortex and at midlatitudes; the calculations fail to reproduce sufficiently strong subtropical tracer gradients. Agreement is best at high latitudes (inside the polar vortex) and is better in the NH than in the SH. Because less meteorological data are available in the

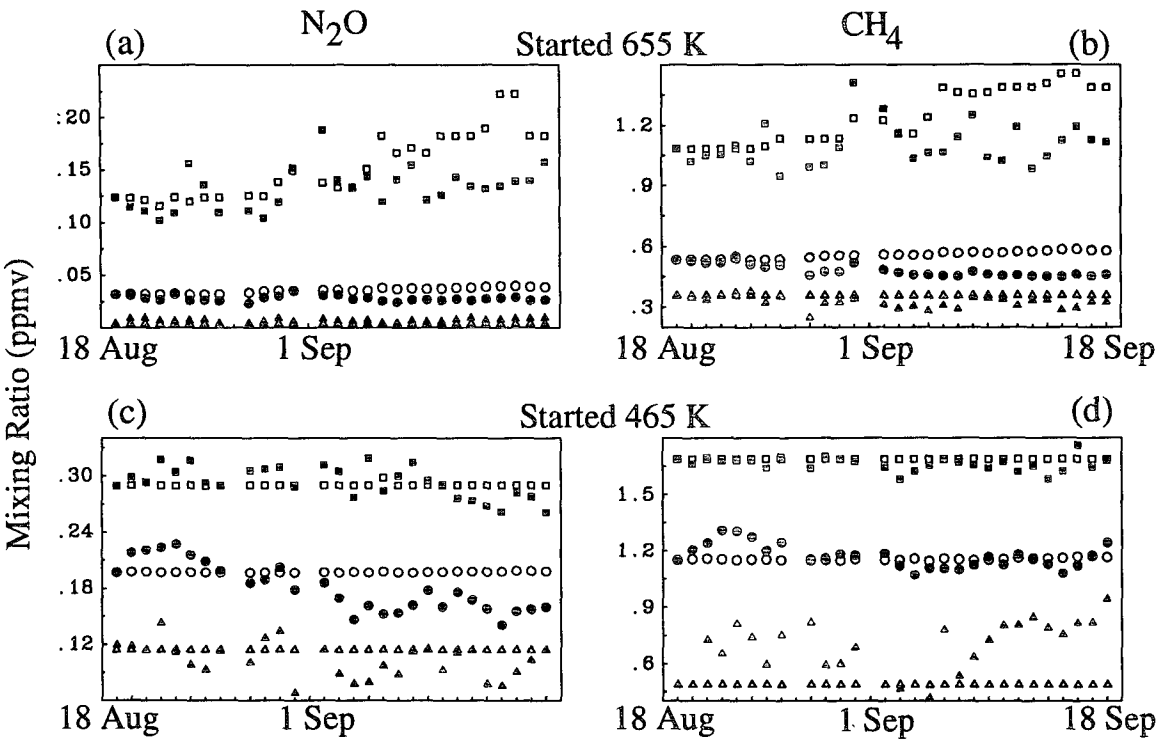

FIG. 21. As in Fig. 14 but for 19 Aug–17 Sep 1992 in the SH; |PV| greater than 1.4×10^{-4} s^{-1} is used in the SH.

SH, the UKMO winds and temperatures are expected to be more uncertain there, and inaccuracies in these would carry through to both the calculated vertical and horizontal motions of the parcels. More-detailed examinations show good agreement of the general patterns of tracer evolution within the vortex. Comparisons of individual parcel values show that the trajectory model tends to result in many parcels with high and low mixing ratios in close proximity in midlatitudes outside the vortex; in some cases the model also fails to reproduce anticyclonic features seen in midlatitudes. Although detailed agreement is lacking here, when calculated fields are averaged, the large-scale patterns of tracer evolution are reproduced. The calculations also show sharper local horizontal gradients along the vortex edge and, during disturbed periods, around the anticyclone. Both effects are due in part to the absence of a parameterization of small-scale mixing in the trajectory calculations. The coarse horizontal resolution of the *UARS* data is also expected to weaken horizontal gradients seen in those observations, and uncertainties in the trajectory calculations are expected to be larger in regions with strong wind shears, such as outside the vortex edge.

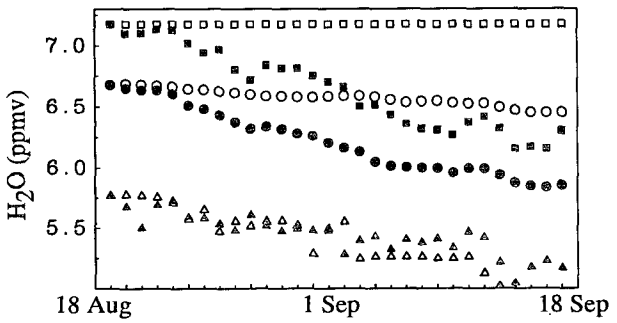

FIG. 22. As in Fig. 21 but for H_2O for parcels initialized at 840 K.

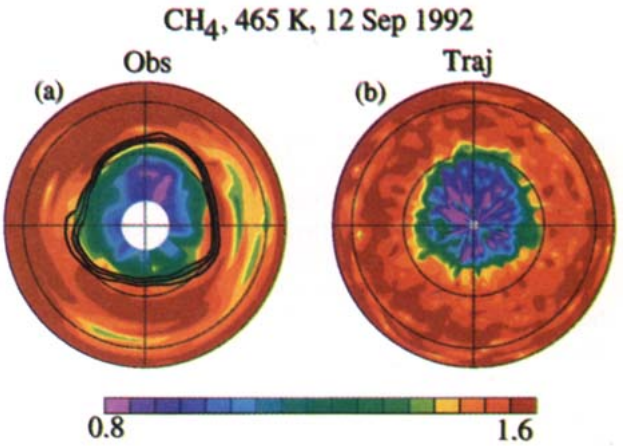

FIG. 23. As in Fig. 7 but for CH_4 at 465 K on day 24 (12 Sep 1992) of the run started 19 Aug 1992 in the SH. The projection is orthographic, with 0° longitude at the top of the plot and 90°E to the right; dashed lines show 30° and 60° latitude circles.

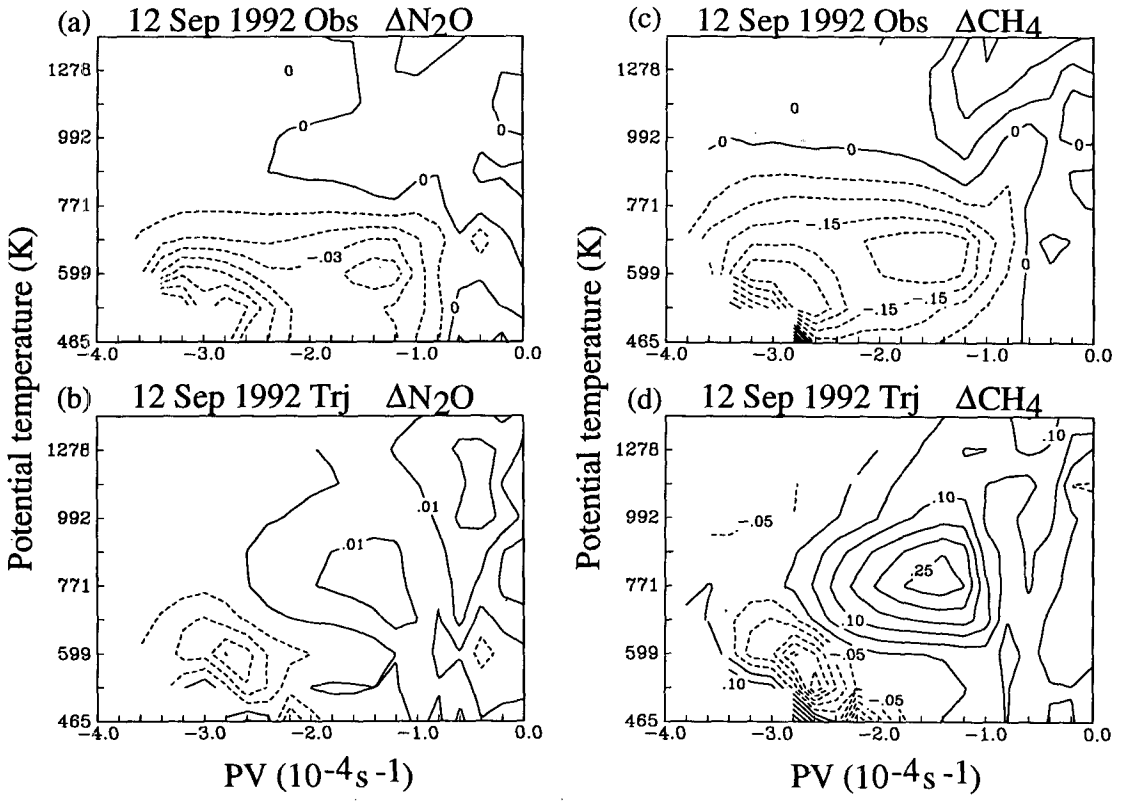

FIG. 24. As in Fig. 12 but on 12 Sep 1992 and for both N_2O (a and b) and CH_4 (c and d).

In the NH late winter, the trajectory model reproduces large tongues of high N_2O that are drawn from low latitudes around the vortex into the region of the anticyclone during February–March 1993. The predicted fields at this time show very narrow tongues of material being drawn off the edge of the vortex into low latitudes and narrow tongues of high N_2O around the edge of the anticyclone. The detection of such narrow features by the low-resolution satellite instruments would depend on the exact measurement locations (e.g., Morris et al. 1995), and we show cases where there is and is not observational evidence of such features. Waugh et al. (1994) showed similar "filamentation" type behavior in very high-resolution contour advection calculations for the Arctic winter stratosphere, and Bowman and Mangus (1993) showed similar filamentation in comparisons of trajectory calculations with total ozone in the SH.

The observed evolution of CLAES N_2O and CH_4 in the SH late winter shows some discontinuities in the lower stratosphere that do not appear to be related to any observed or deduced dynamical changes at that time. Examination of the time evolution of MLS-observed and calculated H_2O shows qualitative differences in the middle and upper stratosphere inside the polar vortex, especially in late winter. MLS H_2O has previously been shown to be useful for identifying and examining the evolution of the polar vortex (Harwood et al. 1993; Lahoz et al. 1994). However, current MLS H_2O retrievals do show apparent nonconservation of H_2O inside the vortex in the middle and upper stratosphere, possibly related to the coarse vertical resolution of the current H_2O retrievals. It is also possible that there could be real nonconservative processes affecting upper-stratospheric H_2O that are not well understood. These features of the evolution of MLS H_2O in the polar middle and upper stratosphere are inconsistent with the expected behavior of a passive tracer and also with the observed behavior of CLAES N_2O and CH_4. The dependence of these inconsistencies on the current retrieval methods is currently under investigation.

The bulk of the evidence shown here suggests that calculated diabatic descent rates are somewhat too strong in the NH midstratosphere and too weak almost everywhere in the SH. Rough estimates of diabatic descent rates in the lower stratosphere indicate that the radiation calculation used in the trajectory code predicts descent rates than are consistent with N_2O and CH_4 observations in the NH. In the NH late winter in 1993, near $\approx$500 K, calculations suggest that $d\theta/dt$ is ≈ -1.0 to -1.4 K/d. These values are comparable to but slightly larger than those given by Schoeberl et al. (1992) for midwinter in the NH in 1989, at a lower level, and for January–March 1993 by Larsen et al. (1994), also at a somewhat lower level. In both early and late winter of the SH lower stratosphere, the cal-

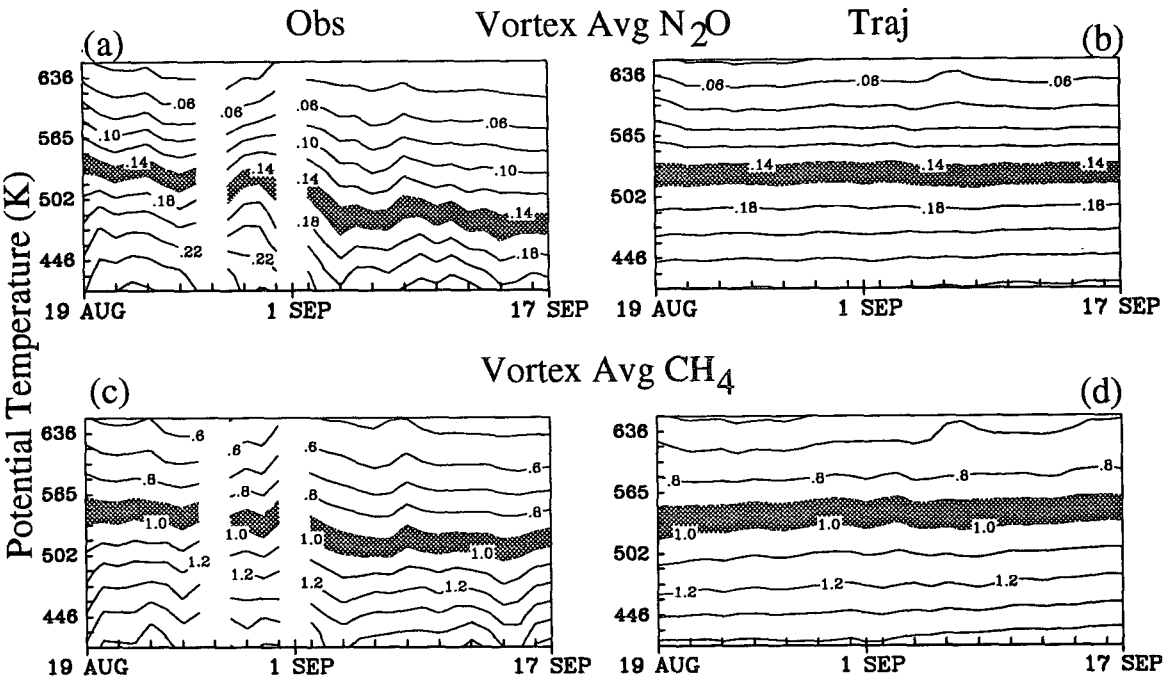

FIG. 25. As in Fig. 20 but for 19 Aug–17 Sep 1992, for the lower stratosphere only, and for both N_2O (a and b) and CH_4 (c and d).

culation predicts smaller descent rates than the observations when averaged over the vortex. In late winter 1992, the range of values suggests that in the SH, between 450 and 500 K, the average descent rate ($d\theta/dt$) is not greater than ≈ -0.4 K/d and is generally confined to a ring along the vortex edge; this is comparable to values given by Schoeberl et al. (1992) for the SH late winter in 1987 and by Schoeberl et al. (1995) for October 1992.

The overall agreement between the calculated and observed long-lived tracer fields indicates that the average characteristics of trajectories calculated using the horizontal winds from the UKMO data assimilation system and computed diabatic vertical (cross isentropic) velocities provide a reasonable approximation to conservative mass transport, at least at the middle and lower stratospheric levels, polar latitudes, and wintertime periods examined here in detail. Although detailed agreement is sometimes lacking in midlatitudes, the large-scale average time evolution is also reasonably well reproduced there. In addition to diagnosing atmospheric motions in a variety of stratospheric contexts, this trajectory approach can provide a baseline against which the evolving distributions of stratospheric trace gases in the polar winter can be examined for nonconservative effects, including the action of photochemistry on shorter-lived trace constituents such as ozone (Manney et al. 1995).

Acknowledgments. We thanks our MLS and CLAES colleagues for their continued collaboration and support; L. S. Elson for providing mapped MLS data; T. Luu for data management; P. A. Newman for routines that were adapted to calculate PV; and M. L. Santee for helpful comments. This research was sponsored by NASA's Upper Atmosphere Research Satellite Project and was performed at the Jet Propulsion Laboratory, California Institute of Technology, under contract with the National Aeronautics and Space Administration.

REFERENCES

Barath, F. T., and Coauthors, 1993: The upper atmosphere research satellite microwave limb sounder instrument. *J. Geophys. Res.*, **98,** 10 751–10 762.

Bowman, K. P., 1993: Large-scale isentropic mixing properties of the Antarctic polar vortex from analyzed winds. *J. Geophys. Res.*, **98,** 23 013–23 027.

——, and N. J. Mangus, 1993: Observations of deformation and mixing of the total ozone field in the Antarctic polar vortex. *J. Atmos. Sci.*, **50,** 2915–2921.

Chen, P., 1994: The permeability of the Antarctic vortex edge. *J. Geophys. Res.*, **99,** 20 563–20 571.

——, J. R. Holton, A. O'Neill, and R. Swinbank, 1994: Quasi-horizontal transport and mixing in the Antarctic stratosphere. *J. Geophys. Res.*, **99,** 16 851–16 866.

Dahlberg, S. P., and K. P. Bowman, 1994: Climatology of large-scale isentropic mixing in the Arctic winter stratosphere from analyzed winds. *J. Geophys. Res.*, **99,** 20 585–20 599.

Dunkerton, T. J., and D. P. Delisi, 1986: Evolution of potential vorticity in the winter stratosphere of January–February, 1979. *J. Geophys. Res.*, **91,** 1199–1208.

Elson, L. S., and L. Froidevaux, 1993: The use of Fourier transforms for asynoptic mapping: Early results from the Upper Atmosphere Research Satellite Microwave Limb Sounder. *J. Geophys. Res.*, **98,** 23 039–23 049.

Eluszkiewicz, J., D. Crisp, R. W. Zurek, L. S. Elson, E. F. Fishbein, L. Froidevaux, J. W. Waters, R. S. Harwood, and G. E. Peckham, 1995: Residual circulation in the stratosphere and lower

mesosphere as diagnosed from Microwave Limb Sounder data. *J. Atmos. Sci.*, in press.

Fisher, M., A. O'Neill, and R. Sutton, 1993: Rapid descent of mesospheric air in the stratospheric polar vortex. *Geophys. Res. Lett.*, **20,** 1267–1270.

Harwood, R. S., and Coauthors, 1993: Springtime stratospheric water vapour in the Southern Hemisphere as measured by MLS. *Geophys. Res. Lett.*, **20,** 1235–1238.

Hsu, C.-P. F., 1980: Air parcel motions during a numerically simulated sudden stratospheric warming. *J. Atmos. Sci.*, **37,** 2768–2792.

Kumer, J. B., J. L. Mergenthaler, and A. E. Roche, 1993: CLAES CH_4, N_2O, and CCL_2F_2 (F12) global data. *Geophys. Res. Lett.*, **20,** 1239–1242.

Lahoz, W. A., and Coauthors, 1993: Northern Hemisphere mid-stratospheric vortex processes diagnosed from H_2O, N_2O and potential vorticity. *Geophys. Res. Lett.*, **20,** 2671–2674.

——, and Coauthors, 1994: Three-dimensional evolution of water vapor distributions in the Northern Hemisphere stratosphere as observed by MLS. *J. Atmos. Sci.*, **51,** 2914–2930.

Larsen, N., B. Knudsen, I. S. Mikkelsen, T. S. Jorgensen, and P. Eriksen, 1994: Ozone depletion in the Arctic stratosphere in early 1993. *Geophys. Res. Lett.*, **21,** 1611–1614.

Loewenstein, M., J. R. Podolske, K. R. Chan, and S. E. Strahan, 1990: N_2O as a dynamical tracer in the Arctic vortex. *Geophys. Res. Lett.*, **17,** 477–480.

Manney, G. L., and R. W. Zurek, 1993: Interhemispheric comparison of the development of the stratospheric polar vortex during fall: A 3-dimensional perspective for 1991–1992. *Geophys. Res. Lett.*, **20,** 1275–1278.

——, L. Froidevaux, J. W. Waters, L. S. Elson, E. F. Fishbein, R. W. Zurek, R. S. Harwood, and W. A. Lahoz, 1993: The evolution of ozone observed by UARS MLS in the 1992 late winter southern polar vortex. *Geophys. Res. Lett.*, **20,** 1279–1282.

——, ——, A. O'Neill, R. Swinbank, J. B. Kumer, J. L. Mergenthaler, and A. E. Roche, 1994a: Stratospheric warmings during February and March 1993. *Geophys. Res. Lett.*, **21,** 813–816.

——, and Coauthors, 1994b: Chemical depletion of ozone in the Arctic lower stratosphere during winter 1992–1993. *Nature,* **370,** 429–434.

——, R. W. Zurek, A. O'Neill, and R. Swinbank, 1994c: On the motion of air through the stratospheric polar vortex. *J. Atmos. Sci.*, **51,** 2973–2994.

——, L. Froidevaux, R. W. Zurek, J. W. Waters, A. O'Neill, and R. Swinbank, 1995: Lagrangian transport calculations using UARS data. Part II: Ozone. *J. Atmos. Sci.*, **52,** 3069–3081.

McIntyre, M. E., and T. N. Palmer, 1984: The 'surf zone' in the stratosphere. *J. Atmos. Terr. Phys.*, **46,** 825–849.

Morris, G. A., and Coauthors, 1995: Trajectory mapping of Upper Atmosphere Research Satellite (UARS) data. *J. Geophys. Res.*, in press.

O'Neill, A., W. L. Grose, V. D. Pope, H. MacLean, and R. Swinbank, 1994: Evolution of the stratosphere during northern winter 1991/92 as diagnosed from U.K. Meteorological Office analyses. *J. Atmos. Sci.*, **51,** 2800–2817.

Pierce, R. B., and T. D. A. Fairlie, 1993: Chaotic advection in the stratosphere: Implications for the dispersal of chemically perturbed air from the polar vortex. *J. Geophys. Res.*, **98,** 18 589–18 595.

——, W. L. Grose, J. M. Russell III, and A. F. Tuck, 1994: Evolution of Southern Hemisphere spring air masses observed by HALOE. *Geophys. Res. Lett.*, **21,** 213–216.

Podolske, J. R., M. Loewenstein, S. E. Strahan, and K. R. Chan, 1989: Stratospheric nitrous oxide distribution in the Southern Hemisphere. *J. Geophys. Res.*, **94,** 16 767–16 772.

Roche, A. E., J. B. Kumer, J. L. Mergenthaler, G. A. Ely, W. G. Uplinger, J. F. Potter, T. C. James, and L. W. Sterritt, 1993: The Cryogenic Limb Array Etalon Spectrometer (CLAES) on UARS: Experiment description and performance. *J. Geophys. Res.*, **98,** 10 763–10 775.

Schoeberl, M. R., and Coauthors, 1989: Reconstruction of the constituent distribution and trends in the Antarctic polar vortex from ER-2 flight observations. *J. Geophys. Res.*, **94,** 16 815–16 846.

——, L. R. Lait, P. A. Newman, and J. E. Rosenfield, 1992: The structure of the polar vortex. *J. Geophys. Res.*, **97,** 7859–7882.

——, M. Luo, and J. E. Rosenfield, 1995: An analysis of the Antarctic Halogen Occulation Experiment trace gas observations. *J. Geophys. Res.*, **100,** 5159–5172.

Shine, K. P., 1987: The middle atmosphere in the absence of dynamic heat fluxes. *Quart. J. Roy. Meteor. Soc.*, **113,** 603–633.

Strahan, S. E., J. E. Rosenfield, M. Loewenstein, J. R. Podolske, and A. Weaver, 1994: The evolution of the 1991-92 Arctic vortex and comparison with the GFDL "SKYHI" general circulation model. *J. Geophys. Res.*, **99,** 20 713–20 724.

Sutton, R. T., H. Maclean, R. Swinbank, A. O'Neill, and F. W. Taylor, 1994: High-resolution stratospheric tracer fields estimated from satellite observations using Lagrangian trajectory calculations. *J. Atmos. Sci.*, **51,** 2995–3005.

Swinbank, R., and A. O'Neill, 1994: A stratosphere–troposphere data assimilation system. *Mon. Wea. Rev.*, **122,** 686–702.

Waters, J. W., L. Froidevaux, W. G. Read, G. L. Manney, L. S. Elson, D. A. Flower, R. F. Jarnot, and R. S. Harwood, 1993a: Stratospheric ClO and O_3 from the Microwave Limb Sounder on the Upper Atmosphere Research Satellite. *Nature,* **362,** 597–602.

——, ——, G. L. Manney, W. G. Read, and L. S. Elson, 1993b: MLS observations of lower stratospheric ClO and O_3 in the 1992 Southern Hemisphere winter. *Geophys. Res. Lett.*, **20,** 1219–1222.

Waugh, D. W., and Coauthors, 1994: Transport out of the lower stratospheric Arctic vortex by Rossby wave breaking. *J. Geophys. Res.*, **99,** 1071–1088.